ELSEVIER

Mechanics of Materials 33 (2001) 371–402

MECHANICS OF MATERIALS

www.elsevier.com/locate/mechmat

Dynamic shear bands: an investigation using high speed optical and infrared diagnostics

P.R. Guduru, A.J. Rosakis *, G. Ravichandran

Aeronautics and Applied Mechanics, Graduate Aeronautical Laboratories, California Institute of Technology, 105-50 Caltech, Pasadena, CA 91125, USA

Received 10 October 2000; received in revised form 27 November 2000

Abstract

This paper presents an experimental investigation of the initiation and propagation characteristics of dynamic shear bands in C300 maraging steel. Pre-fatigued single edge notched specimens were impacted on the edge under the notch to produce shear dominated mixed mode stress fields. The optical technique of coherent gradient sensing (CGS) was employed to study the evolution of the mixed mode stress intensity factors. Simultaneously, a newly developed two-dimensional high speed infrared (IR) camera was employed to observe the temperature field evolution during the initiation and propagation of the shear bands. Possible criteria for failure mode selection are discussed. The IR images, for the first time, revealed the transition of crack tip plastic zone into a shear band and also captured the structure of the tip of a propagating shear band. These thermographs support the notion of a diffuse shear band tip and reveal "hot spots" distributed along the length of a well-developed shear band.

Keywords: Infrared temperature measurement; Failure mode transition; Shear bands

1. Introduction

Ever since Zener and Hollomon (1944) explained the physics of the formation of dynamic shear bands in solids, considerable research effort has been devoted to predict their initiation and to model their structure after they are formed. The generally accepted explanation for their formation is as follows. When solids experience dynamic plastic deformation, most of the external work done is dissipated as heat, which raises the local temperature of the material. When slightly inhomogeneous plastic deformation occurs in an otherwise uniformly deforming material due to the presence of a geometric discontinuity or a material inhomogeneity, and if the deformation is rapid enough to supersede heat conduction effects, local temperature is elevated at those locations of inhomogeneities. This increase in temperature softens the material locally and reduces its resistance to further plastic deformation, i.e., local yield stress is lowered. As a result, plastic deformation becomes more inhomogeneous, leading to a self sustaining cycle of instability: inhomogeneous shear plastic flow – non-uniform temperature distribution – local thermal softening – further inhomogeneous shear plastic flow. The result is the formation of a highly localized shear band, starting from a small non-uniformity of deformation.

* Corresponding author. Tel.: +1-626-395-4523; fax: +1-626-449-6359.

E-mail address: rosakis@atlantis.caltech.edu (A.J. Rosakis).

0167-6636/01/$ - see front matter
PII: S0167-6636(01)00051-5

Thus, the existing inhomogeneities in a structure play a crucial role in precipitating shear bands under dynamic shear loading. Kalthoff and Winkler (1988), in their pioneering experiments, demonstrated that a preexisting notch or a crack can act as an ideal geometric discontinuity in a material to initiate a shear band, when subjected to dynamic shear dominated loading. These experiments are significant because they introduced a new failure mode and a failure mode transition into the framework of dynamic fracture mechanics. In addition, stress and strain fields at a crack tip are analytically well-characterized quantities within the framework of fracture mechanics and the shear band initiation conditions could potentially be described in terms of the well-known fracture mechanics parameters. These experiments initiated numerous efforts to understand the failure behavior of cracks subjected to shear dominated loading and introduced the notion of failure mode transition.

In their experiments, Kalthoff and Winkler (1988) impacted double edge notched specimens of maraging steel with a steel projectile between the two notches, thus generating a shear dominated mixed mode condition at the crack tip. When the impact speed was below a critical value, they observed that cracks initiated in opening mode at an angle of 70° to the crack line. Such a failure mode conforms to the predictions of the well-known mixed mode crack initiation criteria such as the maximum energy release rate criterion and the maximum tensile hoop stress criterion. As the impact speed was increased, a failure mode transition was observed. At high impact speeds, a shear band initiated and propagated from the crack tip. Further, as the crack tip radius was decreased, the critical impact speed required for this transition was also lowered. When the radius was almost zero, i.e., the notch became a fatigue crack tip, within the impact speed range of 20–53 m/s, no opening mode cracks were reported; only shear bands of various lengths were observed. Although they reported a novel failure mode transition for the first time, certain important experimental details, which could help in understanding the mechanics of the failure transition process, were not reported in their work. They include the times of failure initiation in each experiment, and the history of stress intensity factors K_{I} and K_{II} up to initiation (except for two impact speeds, 13 and 33 m/s). Also, in the experiments reported, the angle at which the opening cracks initiated varied from 50° to 70°. Knowledge of the evolution of mode mixity up to crack initiation would provide useful insights into the dynamic mixed mode initiation mechanics. These issues necessitate a detailed experimental investigation in which the stress field at the crack tip is measured continuously up to crack initiation in order to quantify the parameters that govern the competition between the two failure modes, i.e., opening crack and shear band.

Motivated by these experiments, Lee and Freund (1990) carried out theoretical and numerical investigation of the evolution of the mixed mode stress field in a single edge notched specimen, impacted under the notch. Reasonable agreement was found between the predictions of the theoretical analysis and the experimental results reported by Kalthoff and Winkler (1988). The theoretical analysis of Lee and Freund (1990) is valid only until the time when waves reach the crack tip carrying information about the existence of free boundaries and the finite diameter of the projectile. They also performed a numerical analysis of a specimen with a finite geometry. Mason et al. (1992) made an accurate measurement of mixed mode stress intensity factors, evolving with time, in edge notched PMMA specimens, using the optical technique of coherent gradient sensing (CGS) in transmission and high speed photography. They made a detailed comparison between their results and the theoretical and numerical results of Lee and Freund (1990). Good agreement between the three was found at short times. At longer times, the numerical results which accounted for the finite geometry were found to be in better agreement with the experiments than the theoretical results. However, the issue of failure mode transition was not addressed in their investigation.

A detailed study, using a similar specimen geometry and loading arrangement, was conducted by Ravi-Chandar (1995), who tested specimens made of polycarbonate. Dynamic photoelasticity in conjunction with high speed photography was

employed to monitor the evolving stress field around the crack tip. A number of revealing observations were made, which also clarified the findings of Kalthoff and Winkler (1988). It was observed that, when the impact speed was less than 28 m/s, no crack initiated. When the impact speed was between 28 and 32 m/s, an opening crack initiated at an angle of 22° to the crack line after several wave reflections within the specimen. As the impact speed was increased beyond 32 m/s and up to 55 m/s, an opening mode I crack initiated at 68° to the crack line before any reflected waves from the boundaries arrived at the crack tip. This matches very well with the predicted angle of 63° from the analysis of Lee and Freund (1990). Beyond 55 m/s, a shear band initiated and propagated from the crack tip, demonstrating the failure mode transition observed by Kalthoff and Winkler (1988). In addition, Ravi-Chandar et al. (2000) numerically investigated the development of the stress field at the crack tip in order to understand the effect of the impact speed on the mechanics of the failure mode transition. They found that at high impact speeds, formation of a plastic zone in front of the crack tip suppresses the development of high tensile hoop stress at the crack tip which is necessary for a mode I crack to initiate. Thus the impact geometry and the plasticity of the specimen conspire to delay the opening crack failure mode and provide an opportunity for the plastic zone to develop into a shear band. However, the investigations of Ravi-Chandar (1995) and Ravi-Chandar et al. (2000) could not provide the detailed evolution of stress intensity factors because the photoelasticity fringes failed to show any K-dominance. Similar observations of failure mode transition in polymers were also reported by Rittel and Levin (1998). The failure mode transition phenomenon has also been numerically analyzed by Needleman and Tvergaard (1995), who modeled the Kalthoff specimen made of a material, whose response was characterized by an elastic-viscoplastic constitutive relation of a porous plastic solid (Gurson model), with adiabatic heating due to plastic dissipation and the resulting thermal softening accounted for. Like Ravi-Chandar (1995) and Ravi-Chandar et al. (2000), they too noticed that at higher impact speeds, a softening region developing ahead of the crack tip shields the lateral regions from developing high tensile stresses, suppressing the formation of opening cracks.

The above numerical investigations attempted to provide a "mechanism" based explanation for the failure mode transition. They do not provide a criterion to predict failure mode selection. There have been attempts in that direction by formulating criteria in terms of the well-known fracture mechanics parameters such as a critical combination of mode I and mode II stress intensity factors. Zhou et al. (1996b) proposed that a shear band initiates when the J integral reaches a critical value. Chen and Batra (1998a,b,c) proposed that, under adiabatic conditions, a shear band would initiate at a notch or a crack tip when the effective plastic strain at a prescribed distance from the crack tip reaches a critical value. This would translate into a shear band initiation locus on the K_{I}–K_{II} plane for a given mixed mode situation, when the loading is rapid enough to render heat conduction effects negligible. Very limited experimental data is available to test such a hypothesis. The issue is complicated further by another locus on the K_{I}–K_{II} plane which represents failure by opening mode in the form of a kinked crack. Roessig and Mason (1998) examined the shear band initiation behavior of a variety of steels by impacting single edge notched specimens supported against steel dies. They measured shear band initiation times from the experiments. Then, by numerically simulating the experiment, they estimated the critical stress intensity factors at initiation. They found that critical K_{II} can potentially be used to predict the onset of shear bands, though some dependence on impact speed was observed. Rittel and Levin (1998) carried out a series of experiments in which cracks in polycarbonate specimens were subjected to dynamic mixed mode loading. They used a hybrid experimental–numerical technique to investigate the critical conditions at failure initiation. They observed that under different mixed mode conditions, shear bands developed when K_{II} exceeded a threshold value.

All of the contributions discussed above are concerned with the behavior of a notch or a crack

tip when subjected to a predominantly mode II loading in the single/double edge notched geometry subjected to asymmetric projectile impact and the competition between the competing failure mechanisms. However, it should be noted that though the study of the critical conditions for the initiation of a shear band from the tip of a crack subjected to a dynamic mixed mode loading is of special interest within the framework of dynamic fracture mechanics, it is only a particular case of the general problem of initiation of adiabatic shear localization at inhomogeneities or asperities in materials. The question of critical conditions for initiating shear localization in a homogeneously deforming material has received a great deal of attention and there are many excellent references devoted to this topic (Recht, 1964; Rogers, 1979; Clifton, 1980; Bai, 1982; Clifton et al., 1984; Molinari and Clifton, 1987; Shawki and Clifton, 1989; Bai and Dodd, 1992). The study of propagating shear bands is a fascinating subject that has attracted wide attention in the past. From an experimental point of view, the relevant measurable quantities of interest for an advancing shear band are the speed of propagation, its width and the temperature rise along and across the band. Very few detailed investigations have been conducted in the past due to many intractable experimental difficulties associated with such measurements. These difficulties include extremely short duration of the event; typically shear bands initiate and propagate across the region of interest in just a few microseconds, requiring highly repeatable experimental geometries, a measurement device with sub-microsecond response time and very high speed data acquisition systems. Further, shear bands are typically very narrow, often less than 100 μm in width, necessitating measuring devices with extremely high spatial resolution capabilities. In addition, making accurate high speed temperature measurements limits the choice of techniques to infrared (IR) thermography. One of the first attempts to measure the temperature in a shear band using an IR thermographic technique was made by Costin et al. (1979). They subjected thin walled cylindrical specimens to dynamic twisting in a Kolsky torsional bar. Using a single element IR detector, they measured the average temperature over a spot 1 mm in size, that contained a propagating shear band in a low carbon steel and estimated the temperature rise to be about 100°C. Since the spot size was much larger than the width of the shear band, their estimate was a lower bound for the actual temperature rise within the shear band. A more refined investigation, using a linear array of 10 Indium Antimonide (InSb) IR detectors, was conducted by Hartley et al. (1987), for measuring the temperature rise in a shear band in two low carbon steels. The specimens and the loading device were the same as those used by Costin et al. (1979). The detectors measured temperature at 10 discrete points along a line across the projected path of the shear band, as it passed by. They observed that the shear bands in these materials were typically 150–250 μm wide and the maximum temperature rise they measured, using a spot size of 20 μm, was about 450°C. Subsequently, Marchand and Duffy (1988) used a linear array of twelve InSb detectors to measure temperature rise in shear bands in thin walled cylindrical specimens made of HY100 steel. The width of the shear bands in HY100 was typically 10–20 μm. A spot size of 35 μm was used and a maximum temperature rise of about 600°C was reported. Since the spot size was almost twice as wide as the shear band, the measurements were essentially lower bound estimates for the maximum temperature within the band. One disadvantage of using InSb detectors, especially along with small spot sizes, is their low signal to noise ratio. In the above investigations, for example, the temperature resolution was rather low, with the smallest detectable temperature rise being 80°C. Though these experiments were the first comprehensive investigations of the characteristics of adiabatic shear bands, they were limited by the linear arrays of detectors employed. A shear band is essentially a two-dimensional (2-D) entity with a moving tip and an evolving structure behind it and a linear array of detectors can yield only partial information. Using high speed photography, Marchand and Duffy (1988) estimated the speed of the shear band propagation to be around 250–500 m/s. The measurement of the shear band speed was handicapped by the fact that the shear bands initiated at several locations around the circumference of the

specimen and propagated independently to meet each other. A systematic study to investigate the speed of shear bands and the associated temperature rise was undertaken by Zhou et al. (1996a,b) on the single edge notched geometry, with specimens made of a C300 maraging steel. Since they studied shear bands initiating at a notch tip, using a high speed camera, they could clearly image a single propagating shear band and reported propagation speeds up to 1000 m/s. In addition, they also employed a linear array of 16 InSb IR detectors to measure the temperature rise across the shear band. This was the first investigation to measure the shear band speeds accurately and relate them to the impact speeds and to report very high temperatures, close to the melting temperature of the material. These measurements were made over a spot size of 100 μm and thus were limited in spatial resolution. They also observed, for the first time, that for certain impact speeds, a shear band initiates, propagates, arrests within the specimen and a mode I crack initiates from the tip of the arrested shear band at an angle of about 35° to the shear band direction. In addition, they conducted a detailed numerical investigation to simulate the shear band speeds and the failure mode transition. However, the temperatures observed in the experiments were much higher than the computed values.

Analytically, propagating shear bands were investigated, among others, by Wu and Freund (1984), Freund et al. (1985) Wright (1987, 1995), Wright and Ockendon (1992), Wright and Ravichandran (1997) and Grady (1992, 1994). Wu and Freund (1984) sought to investigate the mechanism of shear band formation through the concept of "wave trapping." They considered the problem of a half space whose boundary was subjected to constant shearing velocity. They then analyzed the process by which the information about the boundary conditions is transmitted into the half space and demonstrated how very large strains are accumulated in a thin layer close to the boundary, leading to the formation of a shear band. In order to study the propagation behavior of a shear band, Freund et al. (1985) considered a block of material with a defect and numerically subjected it to antiplane shear deformation. A shear band initiated at the defect and propagated at a speed of $0.57C_S$, where C_S is the shear wave speed of the material. This estimate is higher than the experimentally observed shear band speeds and further experiments are necessary to investigate if shear bands can be driven at higher speeds. Wright and his coworkers, in a series of pioneering articles (Wright, 1987, 1995; Wright and Ockendon, 1992; Wright and Ravichandran, 1997), attempted to model the canonical structure of a well-developed shear band. They developed a theory to describe the structure of temperature, shear strain and strain rate across the shear band. Lack of experimental data regarding temperature and strain rate at such fine length scales has prevented direct experimental verification of these models. Wright and Ravichandran (1997) showed that the theory captures the essential features of the strain distribution across the shear band by comparing it with the experimental results of Moss (1981). Grady (1992, 1994) viewed a shear band as a propagating feature with a well-defined front, containing a process zone where most of the adiabatic heating and stress relaxation occurs. He developed models to predict the length and the width of such a process zone and was able to estimate the rate of energy dissipation within this zone. Once again, lack of experimental data to date at such length scales has prevented direct comparisons. Taking an entirely different point of view, in the single edge notched geometry, Gioia and Ortiz (1996) developed a theory by modeling the shear band as a consequence of the evolving boundary layer between the top and the bottom halves of the specimen. They proposed that within the boundary layer, the unstable shear band is the region where the plastic work exceeds a critical value and as a consequence the tip of a shear band is diffuse in nature, with no singularity associated with it. Their predictions of shear band speeds were in close agreement with those measured by Zhou et al. (1996a).

In the light of the existing body of knowledge, an experimental investigation has been undertaken to address some of the issues discussed above. Detailed measurements of the mixed mode stress intensity factor histories are made and some questions regarding the failure mode transition are

addressed. Using the recently developed IR high speed camera, the 2-D structure of a shear band tip is imaged and the temperature distribution along the shear band is presented. Optical microscopy of certain interesting geometric features of shear bands is also discussed.

2. Experimental techniques

2.1. Material and specimen geometry

In order to study the initiation of a shear band from the tip of a pre-existing crack and its subsequent propagation, a single edge notched specimen geometry, similar to that used by Zhou et al. (1996a), was chosen. This geometry was a modification of the double edge notched geometry used by Kalthoff and Winkler (1988). The specimen geometry and the loading arrangement are schematically illustrated in Fig. 1. The specimen is made of C300 maraging steel, the composition of which is shown in Table 1. The specimens were age hardened by holding them at 482°C for 5 h, followed by air cooling. An electric discharge machining (EDM) notch (260 μm wide) was made on the edge as shown in Fig. 1, which was further extended by 2 mm by fatigue loading. One of the specimen faces was lapped and polished to make it specularly reflective, in order to use it for the optical interference technique of CGS. The specimen is impacted on the edge under the notch, with a 127 mm long cylindrical projectile, 50 mm in diamater, to produce a mixed mode stress field at the crack tip. The projectile is accelerated using a gas gun. The specimen is supported at three points as shown in the Fig. 1. No supports are actually required for the specimen to fail, as demonstrated in the previous experimental investigations. The reason for introducing the supports is to hold the specimen at a fixed location during the loading process, the purpose of which will be discussed in more detail in a later section.

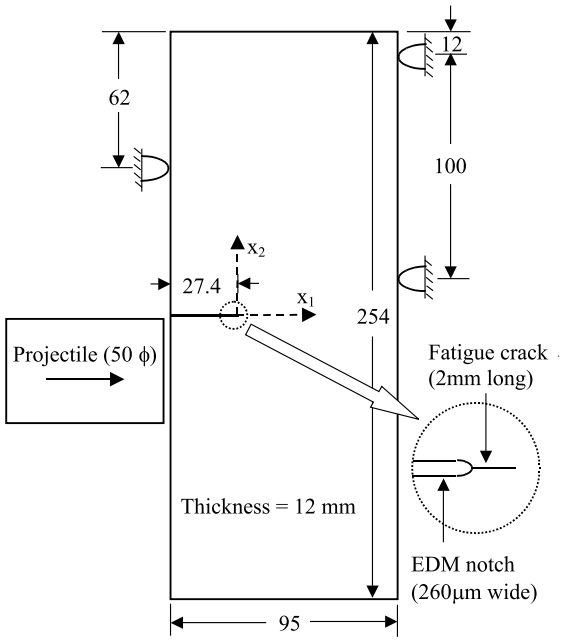

Fig. 1. Specimen geometry and impact arrangement. The projectile is 127 mm long. All dimensions shown are in millimeters.

Table 1
Chemical composition of C-300 maraging steel

Ni	Co	Mo	Ti	Si	Al
18.1	9.1	4.95	0.65	0.08	0.05

In the current investigation, two diagnostic techniques were used to observe the crack tip and the propagating shear band. On one side of the specimen, the optical technique of CGS in reflection was used to monitor the evolution of the stress intensity factors as a function of time. On the other side of the specimen, a newly developed full-field, high-speed IR imaging system was employed to measure the evolving, 2-D temperature field. These techniques are briefly described below.

2.2. Coherent gradient sensing

The optical technique of CGS is a shearing interferometric technique that is sensitive, in reflection mode, to the in-plane gradients of the out of plane displacements. Detailed description of the technique, the equations governing the optical mapping and fringe formation, can be found in the original papers by Tippur et al. (1990, 1991) and in the review article by Rosakis (1993). A schematic illustration of the experimental setup is shown in Fig. 2. The coordinate system used is shown in

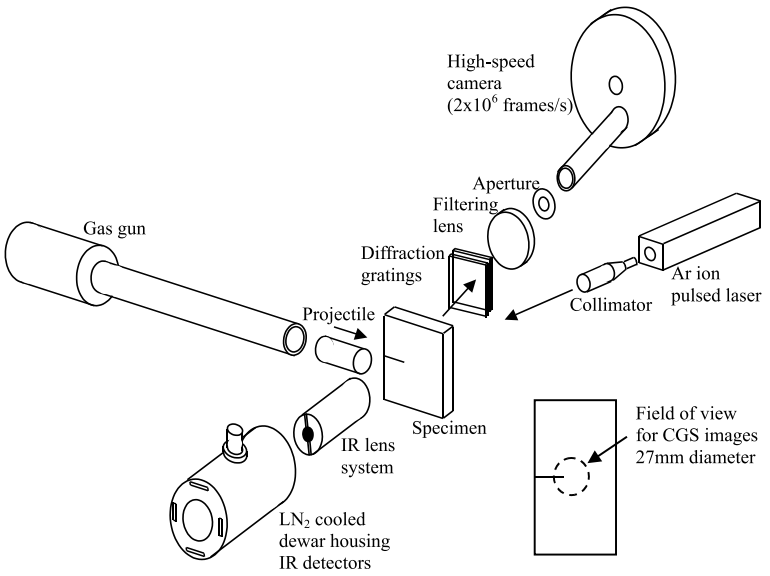

Fig. 2. Schematic illustration of the experimental setup. The CGS setup measures the out of plane displacement gradients on the rear side of the specimen. Simultaneous thermal imaging is accomplished using the IR camera on the facing side of the specimen.

Fig. 1. For opaque materials, this technique involves reflecting a collimated laser beam from the surface of the deforming specimen and optically shearing it by sending it through two high density gratings separated by a distance Δ. This gives rise to multiple diffraction spots of orders $0, \pm 1, \pm 2, \ldots$ and the interference fringe pattern given by the +1 or the −1 order spot is recorded by the imaging system. In the current experiments, the beam has been sheared in a direction perpendicular to the crack. The governing equation for interpreting the interference fringes is

$$u_{3,2} = \frac{\partial u_3}{\partial x_2} = \frac{np}{2\Delta}, \tag{1}$$

where u_3 is the out of plane displacement of the specimen surface, x_2 is the shearing direction of the beam, n is the fringe order and p is the pitch of the gratings, which is 25.4 μm in the current investigation. Thus, each fringe represents the locus of constant $u_{3,2}$ on the specimen surface. Since the fringes are sensitive to the gradients of displacements, they are insensitive to rigid motions of the specimen during deformation, which is one of the distinct advantages of CGS, not shared by other full field optical techniques.

A gas gun accelerates a cylindrical projectile which impacts the specimen edge under the notch as shown. Upon impact, a strain gage attached to the specimen edge triggers an Argon ion laser (Coherent, Sabre Fred) to emit a series of 80 discrete coherent light pulses, (514.5 nm wavelength, 20 ns pulse width) with an inter-pulse time of 2 μs. These pulses are then collimated to a diameter of 50 mm. These pulses pick up information about the out of plane displacement while reflecting on the specimen surface, pass through the CGS setup. The resulting interference fringe patterns are recorded using a rotating mirror type high speed camera (Cordin 330A), capable of framing rates up to 2 million frames per second. The images are recorded on TMAX 3200 high sensitivity film. The field of view of the images was a circle of approximately 27 mm diameter.

2.3. High speed infrared thermography

2.3.1. Two-dimensional infrared imaging system

IR thermography has been used for measuring temperature rise in dynamic deformation and failure experiments by many investigators in the past (Moss and Pond, 1975; Costin et al., 1979; Hartley

et al., 1987; Marchand and Duffy, 1988; Zehnder and Rosakis, 1991, 1992; Mason and Rosakis, 1993; Zehnder et al., 1993; Kallivayalil and Zehnder, 1994; Zhou et al., 1996a; Guduru et al., 1998; Li and Lambros, 2000; Hodowany et al., 2000). All the investigations conducted so far have utilized either a single element detector or a linear array of detectors. Using a linear array of detectors, it is possible to measure temperature at a series of discrete points along a line on the specimen surface. Such detectors have been successfully used by Zehnder and Rosakis (1991) and Mason and Rosakis (1993) to measure the temperature rise across a propagating opening crack in a high strength steel. Costin et al. (1979), Hartley et al. (1987), Marchand and Duffy (1988) and Zhou et al. (1996a) used them to measure the temperature rise across a propagating shear band in steels. However, the linear arrays of detectors are ideal to measure temperature distribution across features that are essentially one-dimensional (1-D) and steady. Although a great deal of information can be obtained with the linear arrays of high speed IR detectors, given the highly transient 2-D nature of the shear band tip and the significance of its structure in understanding the mechanics of shear bands, it would be desirable to have an instrument that can measure dynamically varying temperature field in an area instead of at points along a line. Since several events involving dynamic deformation in solids occur at time scales of tens of microseconds, such measurements can be accomplished using a 2-D square array of IR detectors acquiring images at rates of around 1 MHz.

Although there have been great advances in 2-D IR imaging systems in recent years, there are no commercial systems capable of imaging at such high speeds. IR imaging systems typically run at television rates, 30 Hz, although higher speed systems do exist, with rates of up to 34 kHz. To achieve the required framing rates of up to 1 MHz requires very fast and temporally frozen data acquisition in conjunction with a high-speed 2-D IR detector array. The bottleneck in performing such measurements has been data acquisition. However, utilizing the fast, relatively inexpensive digitizers which are now available, a 2-D IR imaging system has recently been designed and built at Caltech. This instrument, for the first time, enabled the measurement of thermal fields at rates of up to 1 million frames per second. The complete imaging system, consisting of the focusing optics, IR focal plane array, multiplexing circuits, and data acquisition boards is shown in the block diagram of Fig. 3. At the heart of the system is an 8×8 focal plane array of HgCdTe IR detector elements. Each detector element is 100 μm × 100 μm, with center to center spacing of 130 μm.

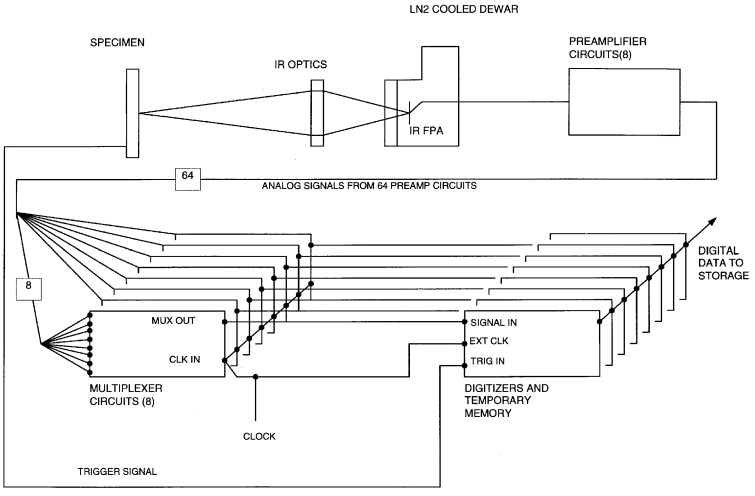

Fig. 3. Block diagram for IR camera operation.

Each of the 64 elements has its own preamplifier, the outputs of which are fed into a bank of eight 8:1 multiplexers. The multiplexed signals are then digitized using four 2-channel, Gage 1012 A/D boards, running at speeds up to 10 MHz. Radiation emitted from the object as it deforms and heats up is focused onto the IR focal plane array using a reflective lens, built up out of two Schwarzschild objectives, each operating at infinite conjugation ratio. The ray diagram for the focussing optics is shown Fig. 4. A photograph of the camera is shown in Fig. 5. The magnification of each lens is fixed and to achieve different magnifications, different lenses are used. In the current investigation, a magnification of 0.9 was used. At this magnification, each detector would be measuring the average temperature over an area of 110 μm × 110 μm. In this system, there is no integration of the signal between frames as in commercial IR cameras; thermal resolution is sacrificed in favor of speed. The system rise time is approximately 750 ns. The details of each of the components of the system and the results of some preliminary applications of the system are given in Zehnder et al. (2000). In order to convert the voltage signals from the detectors to the corresponding temperatures, an output signal vs. temperature rise calibration curve is obtained for the detectors.

2.3.2. IR system calibration

Calibration of the system is performed in a direct manner. A sample of the same material and surface finish as will be tested is heated in an oven by several hundred degrees. The heated sample, instrumented with a thermocouple to record its surface temperature, is placed in the object position. As the sample cools, the voltage output from each of the IR elements is recorded by the data acquisition system along with the sample

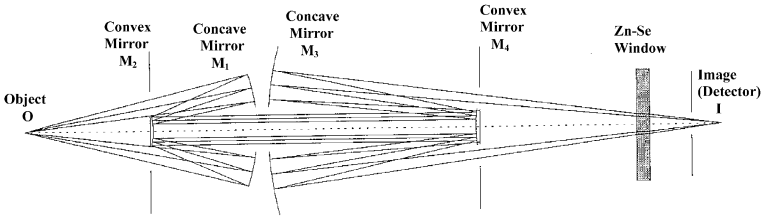

Fig. 4. Ray diagram for double Schwarzchild optical focussing lens.

Fig. 5. A photograph of the IR camera.

temperature. This procedure provides a voltage vs. temperature curve for each element. Since the IR system is AC coupled, the input radiation to the detectors must contain an AC component. This is achieved by placing a chopping wheel in front of the heated calibration specimen.

Great care should be taken during the calibration procedure since any errors made at this stage are directly reflected in the final measurements. Further, oxidation of the sample surface when heated to high temperatures during calibration changes its emissivity substantially, rendering the calibration curve inapplicable. The ideal way to overcome the oxidation problem is to perform the calibration in vacuum or in an inert gas atmosphere, both of which are experimentally cumbersome procedures. As an alternative, the following procedure has been adopted. First, the sample was heated up to a temperature at which no oxidation takes place on its surface, about 225°C in this case, and a calibration is performed while it cools down to room temperature. In order to verify that indeed no oxidation has taken place, the same sample, without modifying the surface condition in anyway, is heated repeatedly to 225°C and the calibration curves are obtained. The curves obtained in four such repetitions, for one of the 64 detectors, are shown in Fig. 6. The proximity of all of them to each other confirms that there was no oxidation up to 225°C. Next, the specimen was heated to a higher temperature, about 525°C and a calibration was performed while the specimen cooled down. This curve, along with the curve obtained by heating the specimen up to 225°C, is shown in Fig. 7. The ratio of these curves to each other represents the ratio of the emissivities of the two surfaces. This ratio is plotted as a function of temperature rise in Fig. 8. It can be seen that this ratio, after some initial non-linearity, settles down to a constant value of 1.55, which is essentially the ratio of the emissivity of the oxidized surface to that of the non-oxidized surface. The calibration curve corresponding to the non-oxidized surface is then extended to higher temperatures by simply dividing the calibration curve of oxidized surface by the factor 1.55. It should be noted that during a dynamic experiment, the temperature elevations of

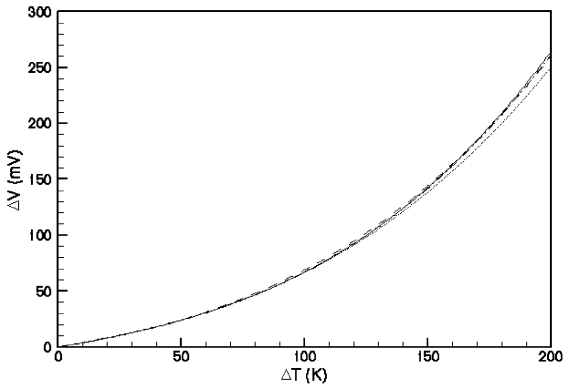

Fig. 6. Calibration curves obtained by repeatedly heating the sample to 225°C.

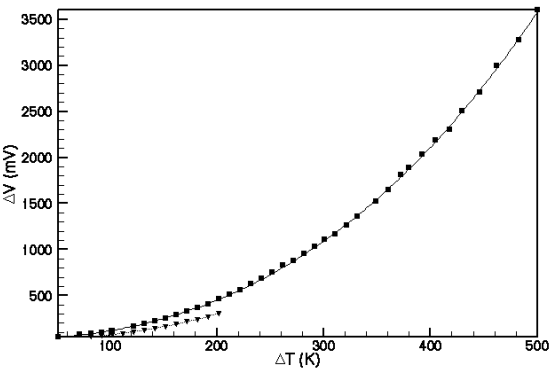

Fig. 7. Calibration curves obtained by heating the sample to 525°C and 225°C.

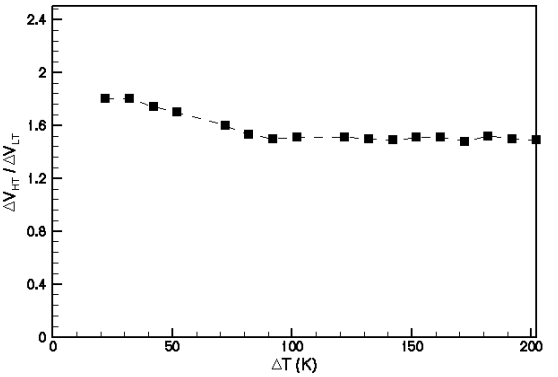

Fig. 8. Ratio of the two calibration curves shown in Fig. 8. ΔV_{HT} is the output from the 525°C test and ΔV_{LT} is the output from the 225°C test.

interest happen at such short time intervals that no oxidation has the time to build up during the observation window.

2.4. Specimen support and triggering

Another important issue where great care should be taken while making temperature measurement is in properly supporting the specimen. Traditionally, the edge impacted specimens for studying shear bands are not supported since failure initiates within the first few reflections of the stress waves emanating from the impact site. However, the initial stress waves impart a translation velocity to the specimen in the direction of impact. Usually, the time window of temperature measurement at a specific area on the specimen surface, such as at the crack tip, following the impact is of the order of 100 μs. If the projectile impacts the specimen at a speed of 35 m/s, and assuming that the characteristic translation speed of the specimen has a similar magnitude, the specimen travels a distance of 3.5 mm during the time of measurement. Hence, each detector would measure temperature not at a particular targeted point on the specimen, but at a series of points along a line as they travel across the field of view of the IR camera. In order to ensure that each detector measured temperature at the same location, the specimen was supported at three points as shown in Fig. 1, preventing translations and rotations. These supports would certainly affect the evolution of the stress intensity factors at long times but would not have any effect during the first 30–40 μs, before the reflected waves from the supports reach the crack tip.

During the experiment, the same strain gage on the specimen, which upon impact triggers the laser pulses, also triggers the data acquisition system for the IR camera, initiating thermal image acquisition. The specimen was impacted at speeds ranging from 10 to 38 m/s. The primary objectives of IR imaging in the current investigation were to image the development of the plastic zone at the pre-existing crack tip and its transition to a shear band, to image the temperature structure of the tip of a propagating shear band and to investigate the temperature distribution along such a band. In order to observe the plastic zone, the IR camera was focussed at an area around the fatigue crack tip and in order to investigate the structure of the propagating band, the area of observation was located 3.5 mm in front of the crack tip, along the expected path of the shear band.

3. Experimental results

3.1. Failure modes

The experiments conducted can be divided into four groups. (i) Those in which the impact speed (v) was less than 13 m/s. A crack tip plastic zone was observed and there was no crack initiation. (ii) 13 m/s $< v <$ 26 m/s. In this speed range, the crack initiated in opening mode, at an angle to the crack line, after several wave reflections. (iii) 26 m/s $< v <$ 32 m/s. In these experiments, a shear band initiated, propagated and arrested within the specimen. This was followed by a failure mode switching to an opening crack from the tip of the arrested shear band at an angle to the shear band direction. (iv) $v >$ 32 m/s. At these high impact speeds, the shear bands propagated through the entire width of the specimen. Some illustrative cases will be examined in the following section in detail.

3.2. Stress intensity factor history when $v < 26$ m/s

When the impact speed was below 13 m/s, no macroscopic failure initiation was observed. However, beyond 13 m/s, a crack initiated in locally opening mode at an angle to the initial crack line. A sequence of CGS images illustrating the history of mixed mode stress field from impact until crack initiation is shown in Fig. 9, from the experiment with an impact speed of 15.5 m/s. The pictures have a black rectangular patch on them, which is a scale marker stuck on the specimen surface. The images show a mixed mode field, consisting of compressive mode I and shear mode II components, building in magnitude up to 76 μs, as demonstrated by the increasing size of the fringes. Also, the fringes are seen to rotate, indicating a shift towards a higher mode I stress

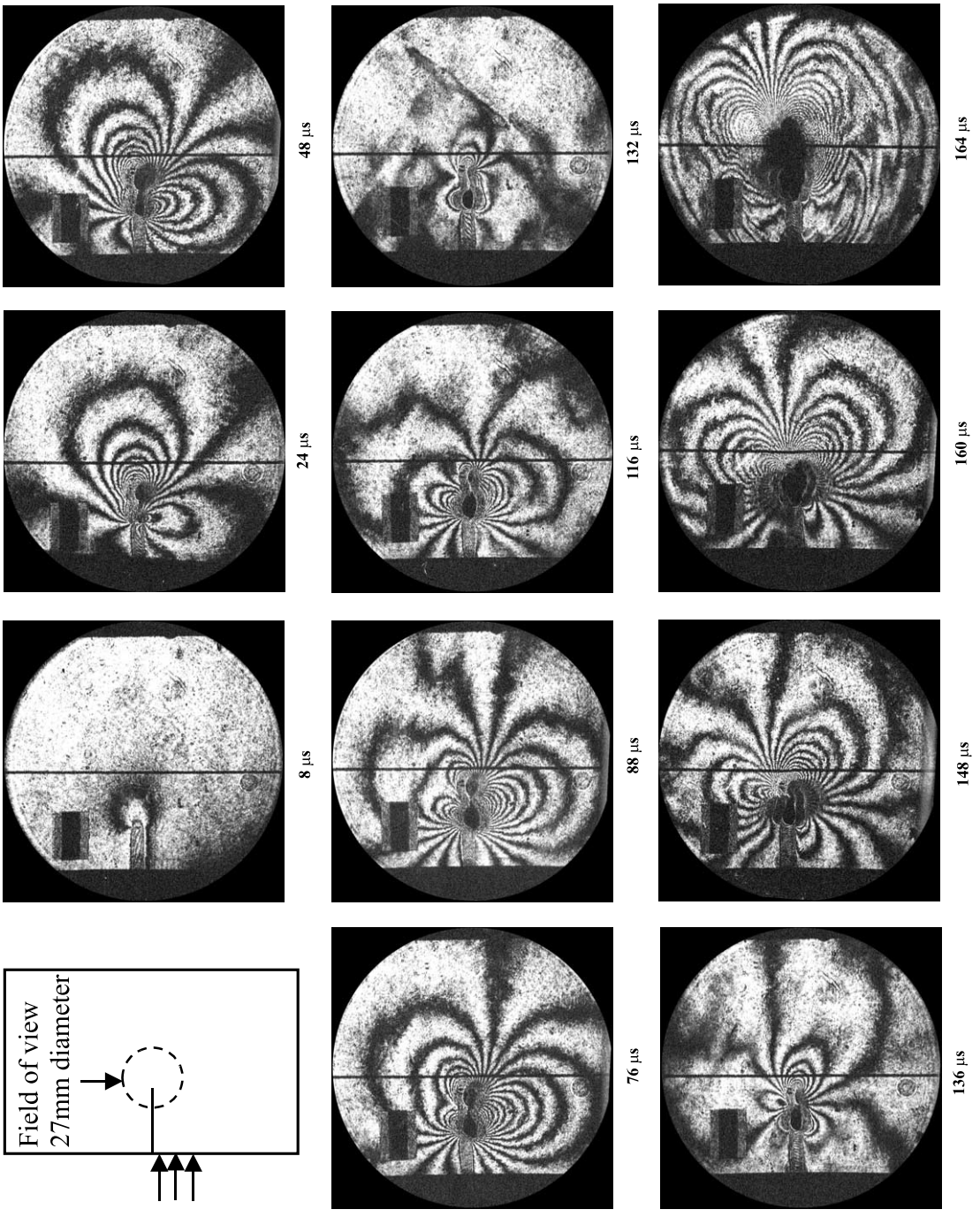

Fig. 9. A sequence of CGS images obtained from the experiment with an impact speed of 15.5 m/s.

intensity factor. Beyond 76 μs, the stress intensity factors are seen to decrease and become almost zero around 132 μs. This is followed by a build up of a mixed mode field, comprised of a tensile opening stress field and a shear stress field. At 164 μs, critical conditions for crack initiation under mixed mode conditions are reached and the initiated crack, along with the waves released in the initiation process, can be discerned in the last image of Fig. 9. When the impact speed is less than 13 m/s, the stress intensity factors do not build up enough to cause crack initiation. Before attempting to devise an appropriate way to extract the stress intensity factors from the fringes, it is essential to understand the actual stress state at the crack tip in the presence of a fatigue crack tip.

According to the analysis of Lee and Freund (1990), when a single edge notched specimen is impacted under the notch, like in the current experiment, the resulting stress field at the crack tip would be mixed mode in nature, though shear dominated. The mode I stress intensity factor K_I would be negative. If the crack faces are separated initially, as in the case of a notch, the compressive part of the stress field brings the two crack faces closer to each other. In addition, two points, one on each face of the crack, both initially located at equal distance from the notch tip, would also slide with respect to each other along the crack direction, due the shear component of the notch tip stress field (K_{II}). This is illustrated in Fig. 10(a). The point O is the notch tip and it is the origin for the singular stress fields. Now let us examine the case of a mathematically sharp crack, all along its length, subjected to the same impact loading. This is illustrated in Fig. 10(b). Since the crack faces are already in contact, they can not be brought any closer and thus, no negative mode I stress intensity factor K_I can develop, rendering K_I to be identically zero. Thus, there can be only sliding of one face relative to the other, which means that there can only be a mode II stress intensity factor K_{II}. This K_{II} is clearly a combined result of the applied boundary load and the frictional traction distributed along the crack faces. And this is also the stress intensity factor that is experienced by the material in front of the crack tip and governs the failure processes therein. Any optical technique that is based on measuring the field quantities such as the out of plane displacement or its gradient, such as the CGS, measures the value of this net K_{II}. As an extreme example, if the frictional locking is severe enough to prevent any relative sliding, then the frictional traction developed along the crack faces would be such that it would produce a K_{II} which is exactly equal in magnitude but opposite in sign to that produced by the boundary loading, to render the net stress intensity factor at the crack tip to be identically zero.

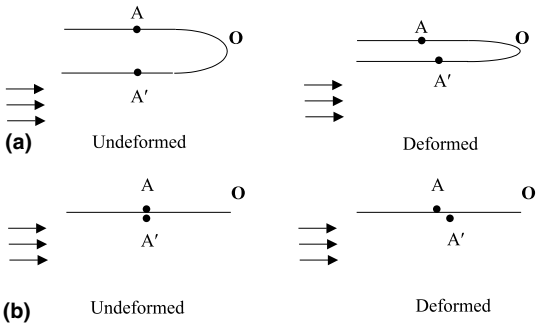

Fig. 10. Schematic illustration of (a) notch tip loading and (b) sharp crack tip loading.

Now let us turn to the events at the notch tip with a fatigue precrack. Along the fatigue crack, the crack faces are already in contact. This is illustrated in Fig. 11. O is the notch tip, and O′ is the fatigue crack tip. After the waves from the impact site arrive, the crack tip area is deformed as illustrated in Fig. 11(b). Points A and A′ come closer to each other as well as slide with respect to each other. Points B and B′ can only slide with respect to each other. This situation can be described as the combination of the two loading scenarios illustrated in Fig. 11(c) and (d). Since the crack faces can come close to each other only to the left of point O, there would be a compressive mode I singular stress field with O as its origin and there will be a mode II singular field with O′ as the origin. The net stress intensity factor K_{II} acting on the material at O′ is the combination of the boundary loads and the distributed frictional traction on the fatigue crack faces. Thus, stress at a point P in Fig. 11(e) can be described as

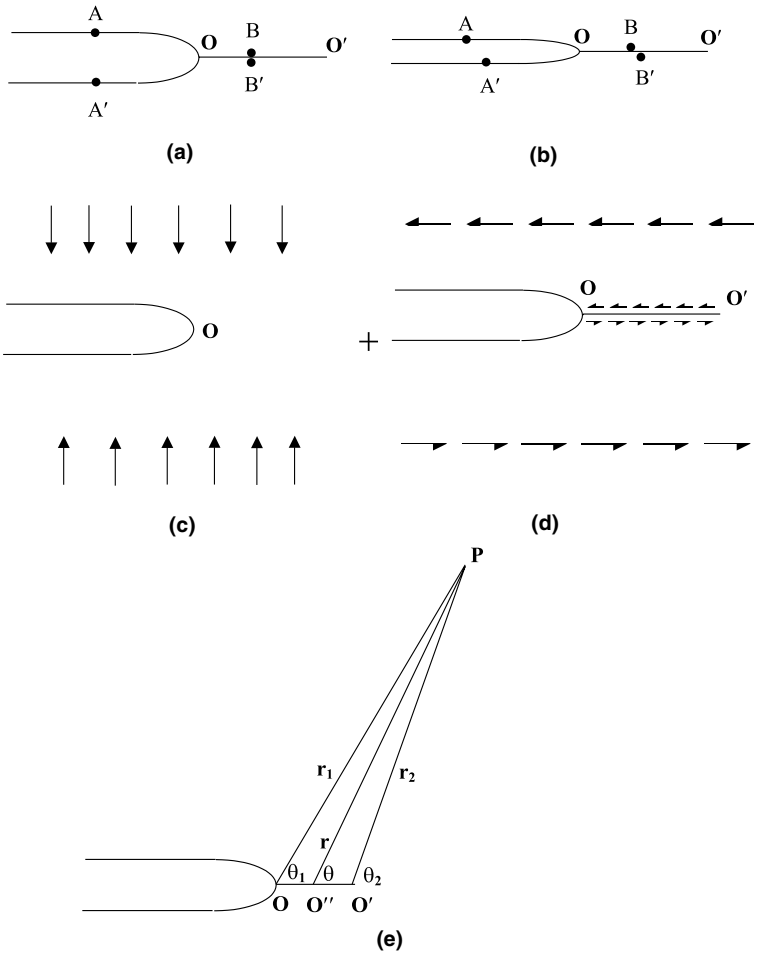

Fig. 11. Schematic illustration of loading of a notch top with an extended fatigue crack: (a) undeformed; (b) deformed; (c) compressive K_{I}; (d) shear K_{II}.

$$\sigma_{ij}(r_1, r_2, \theta_1, \theta_2) = \frac{K_{\mathrm{I}}}{\sqrt{2\pi r_1}} f_{ij}^{\mathrm{I}}(\theta_1) + \frac{K_{\mathrm{II}}}{\sqrt{2\pi r_2}} f_{ij}^{\mathrm{II}}(\theta_2), \tag{2}$$

when K_{I} is negative. $r_1, r_2, \theta_1, \theta_2$ are defined in Fig. 11(e). σ_{ij} are the components of stress, and f_{ij}^{I} and f_{ij}^{II} are known angular functions. K_{I} is the stress intensity factor for the mode I compressive singular field which acts with O as its origin and K_{II} is the stress intensity factor for the mode II singular field which acts with O′ as its origin. It should be remembered that the above description would be valid only when the distance between O and O′ is small compared to the characteristic length of the region over which a single parameter description of the singular field is reasonable. When the mode I component of the stress field is positive, i.e., opening, naturally, O is the origin for both components of the singular field and the stress at the point P can be described as

$$\sigma_{ij}(r_2, \theta_2) = \frac{K_{\mathrm{I}}}{\sqrt{2\pi r_2}} f_{ij}^{\mathrm{I}}(\theta_2) + \frac{K_{\mathrm{II}}}{\sqrt{2\pi r_2}} f_{ij}^{\mathrm{II}}(\theta_2). \tag{3}$$

Using, Eq. (2), the governing Eq. (1) for analyzing the CGS fringes reduces to

$$\frac{np}{2\Delta} = \frac{vh}{2E\sqrt{2\pi}}\left[K_{\mathrm{I}} r_1^{-3/2}\sin\frac{3\theta_1}{2} + K_{\mathrm{II}} r_2^{-3/2}\cos\frac{3\theta_2}{2}\right], \tag{4}$$

where n is the fringe order, p is the pitch of the gratings, Δ is the distance between the gratings, v is the Poisson's ratio, h is the specimen thickness and E is the specimen Young's modulus. The fringes are digitized and the above equation along with the least squares procedure, described by Mason et al. (1992), is used to extract K_{I} and K_{II}. In order to verify the accuracy of the calculation procedure, the extracted K_{I} and K_{II} are used to generate synthetic CGS fringes, which are compared with the experimental fringes, as illustrated in Fig. 12. The good agreement between the two testifies to the accuracy of the procedure. It should be noted that the artificial fringes are able to reproduce the structure of the fringes close to the crack tip, which is a consequence of using two origins O and O′ for the mode I and mode II singular fields, respectively. However, since the length of the fatigue crack is only 2 mm, if the digitized fringes are sufficiently far away from the crack tip, calculation of K_{I} and K_{II} as described above would not be very different from a calculation based on just one origin, such as O″ in Fig. 11(e), for both singular fields. The stress intensity factors have been computed employing both methods for a few cases and the difference between the stress intensity factors obtained was less than the estimated errors in their calculation, though the latter approach would not be able to reproduce the fringe patterns very near the crack tip as good as the former.

Fig. 13 presents the evolution of the normalized K_{I} for four different experiments as a function of normalized time. The normalizing parameter K' is the same as that used by Mason et al. (1992),

$$K' = \sqrt{\frac{l}{\pi}}\frac{Ev}{2c_{\mathrm{d}}^{\mathrm{pl}-\sigma}},$$

where l is the initial crack length, v is the impact speed and $c_{\mathrm{d}}^{\mathrm{pl}-\sigma}$ is the plane stress dilatational wave speed. Time is normalized with $l/c_{\mathrm{d}}^{\mathrm{pl}-\sigma}$. Fig. 14 shows the evolution of K_{II} for the same four experiments. The normalizing factors used are the same as those used for K_{I}. A closer examination of the data at early times allows comparison with the analytical and numerical results of Lee and Freund

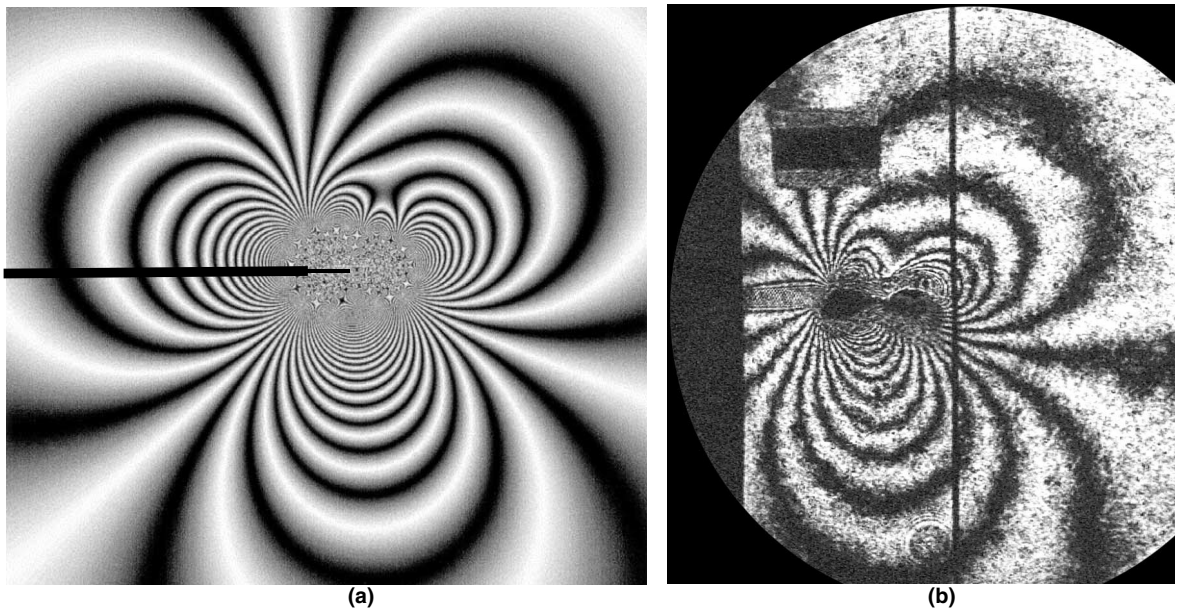

Fig. 12. Comparison between synthetic and experimental fringes.

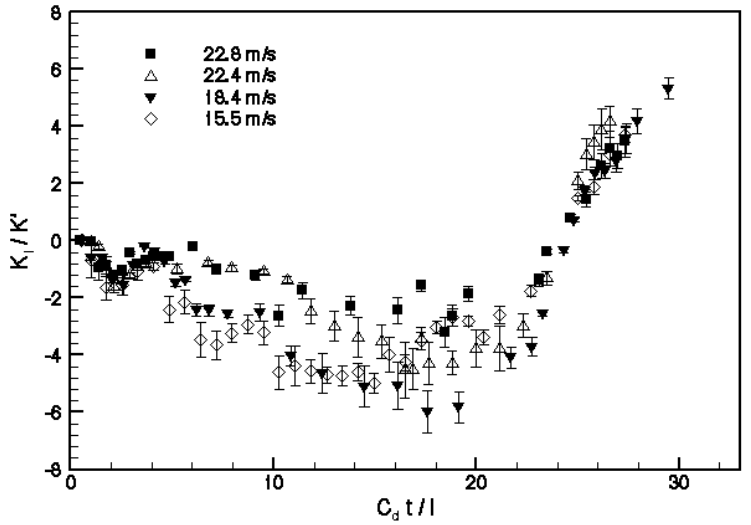

Fig. 13. Evolution of K_I prior to crack initiation in opening mode.

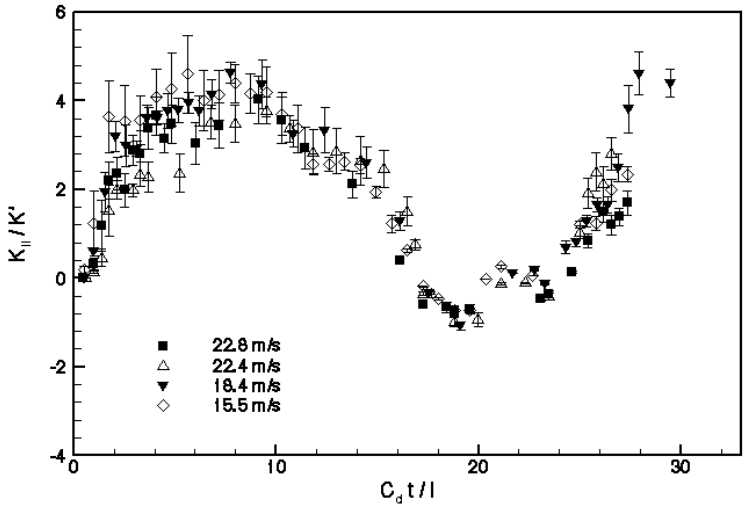

Fig. 14. Evolution of K_{II} prior to crack initiation in opening mode.

(1990) and the previous experimental results of Mason et al. (1992). These comparisons for K_I and K_{II} are shown in Figs. 15 and 16, respectively. The agreement is very good for K_{II} and is reasonably good for K_I. The differences could be attributed to the presence of the fatigue crack. The value of K_{II} peaks around a normalized time of 10 and reaches a minimum around 20. These values are most likely related to the length of the projectile which is approximately five times the length of the crack, l, and hence the length of the loading pulse is $10l$. The magnitude and the time period of the oscillation in K_{II} and K_I are in good agreement with the numerical simulations of Rittel and Levin (1998) and Roessig and Mason (1998) despite the difference in the boundary conditions.

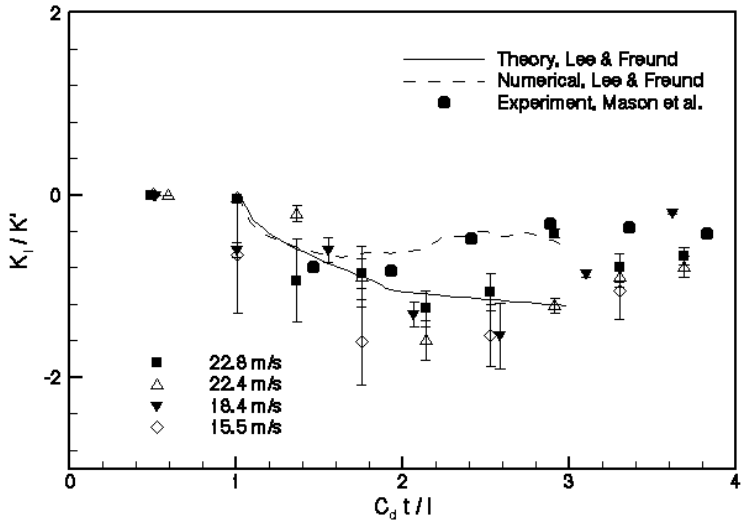

Fig. 15. Comparison of K_I evolution with analytical and numerical solutions of Lee and Freund (1990) for short times.

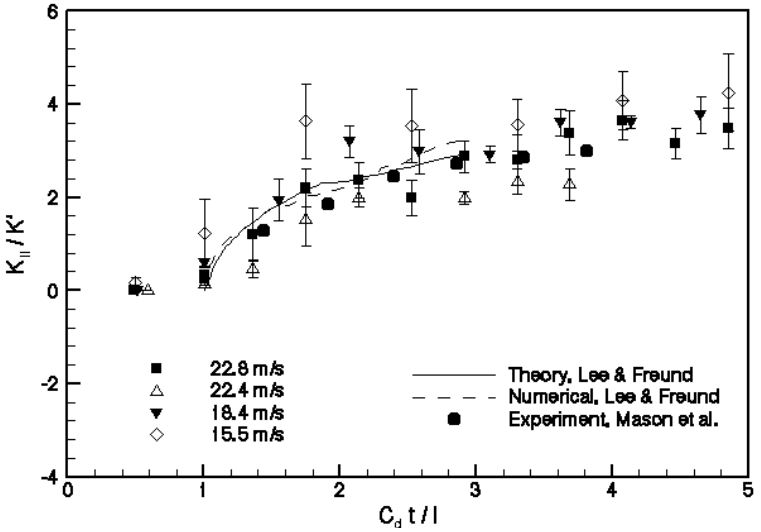

Fig. 16. Comparison of K_{II} evolution with analytical and numerical solutions of Lee and Freund (1990) for short times.

3.3. Incipient shear banding when $v < 26$ m/s

When the projectile speed was less than 26 m/s, though the crack initiated in an opening mode at an angle to the crack line, a microscopic examination of the crack tip area reveals a small and thin arrested shear band at the tip of the initial crack. This was observed in all experiments with impact speeds ranging from 10 to 26 m/s. An optical micrograph of the sample from the crack tip area, polished and etched, is shown in Fig. 17. The arrested shear band can be seen as a thin white band. The length of the band varied from one experiment to another and the longest observed was about

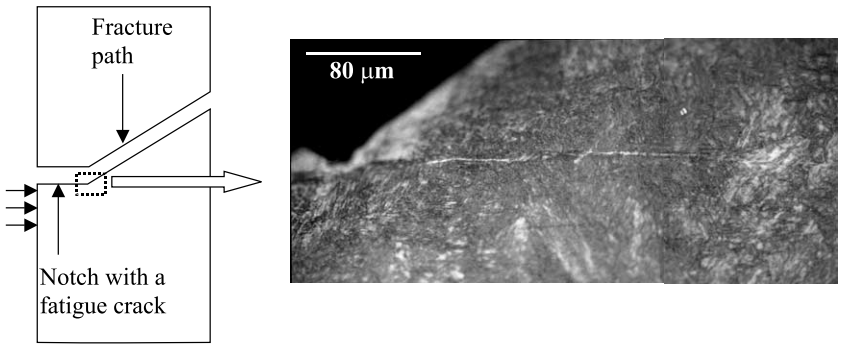

Fig. 17. An optical micrograph of an incipient shear band at the crack tip.

0.5 mm. Examining the history of K_{II}, it can be concluded that this band initiated around or before a normalized time of 10, when the magnitude of K_{II} reached a peak value. Assuming that an increasing K_{II} provides the driving force for the shear band to propagate, it would have arrested when K_{II} started to decrease. Subsequent wave reflections would result in a mixed mode field with a strong opening mode I component, leading to crack initiation in opening mode. Based on this observation, it appears that the failure mode transition has a significantly different connotation in this material from the traditional view and will be discussed in a subsequent section.

3.4. Stress intensity factors when $v > 26$ m/s

When the impact speed is greater than 26 m/s, a shear band initiates and propagates from the tip of the crack. A sequence of CGS images leading up to the initiation of shear band is shown in Fig. 18, for the case where the impact speed was 38 m/s. The shear band initiation can be identified by the elongated dark region at the crack tip, which continues to propagate in the subsequent images. The fringe patterns up to initiation are analyzed in the same way as described above. The stress intensity factors increase rapidly and the critical values of K_I and K_{II} at the time of initiation for six different experiments are shown in Figs. 19 and 20, respectively. From Fig. 20, it appears that there is a critical range of K_{II}, within which the shear band initiates from a pre-fatigued initial notch. Chen and Batra (1998a,b,c) proposed that since the stress intensity factors determine the stress and strain fields near the crack tip, they could potentially be used to formulate a criterion for shear band initiation under adiabatic conditions. Based on hybrid techniques, such a suggestion was also made by Roessig and Mason (1998) and Rittel and Levin (1998). Data presented in Fig. 20 seems to support such a proposal. From Fig. 19, it appears that the value of K_I at initiation may not have a significant role in determining the critical conditions, possibly because it represents a compressive singular field about the notch tip O and not the fatigue crack tip O′. The critical K_{II} criterion gains further support if the results of Fig. 20 are combined with the peak K_{II} values of the experiments with $v < 26$ m/s, as shown in Fig. 21. As discussed in the previous section, if it is assumed that the arrested incipient shear bands which appeared in those experiments, initiated close to the peak value of K_{II}, then irrespective of the subsequent propagation history, a shear band appears to have initiated within a narrow range of K_{II} values. However, this result should be qualified by stating that shear bands are extremely sensitive to the geometry of the inhomogeneities at which they are initiated, in this case, a fatigue crack tip. Thus, a substantial change in critical K_{II} could be expected if a notch tip was used instead of a sharp fatigue crack tip.

3.5. Shear band propagation speed

Fig. 22 shows a sequence of CGS images illustrating the propagation of the shear band follow-

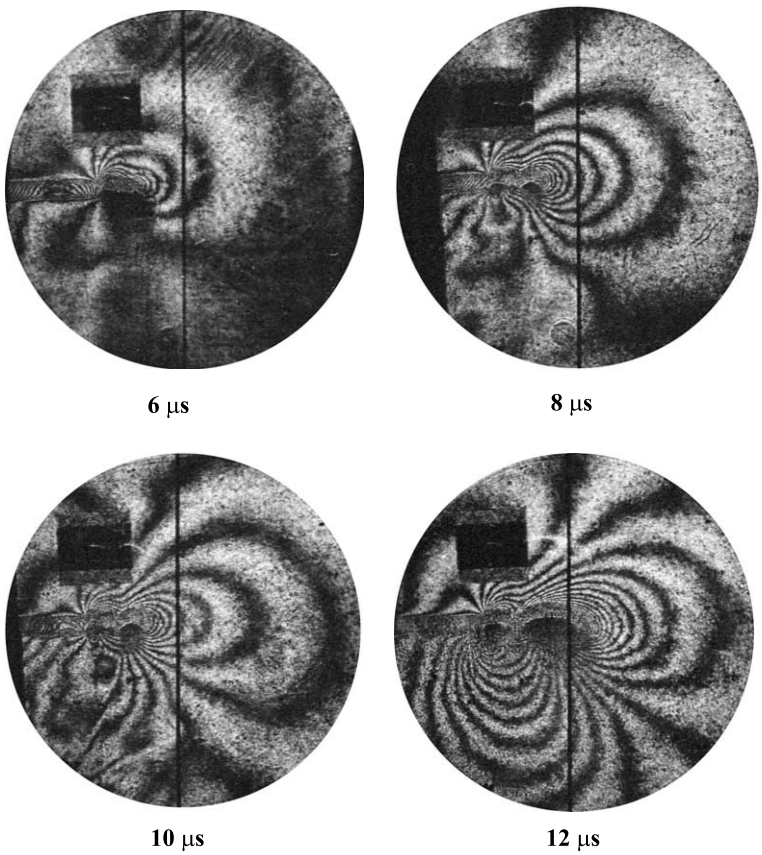

Fig. 18. A sequence of CGS images up to shear band initiation.

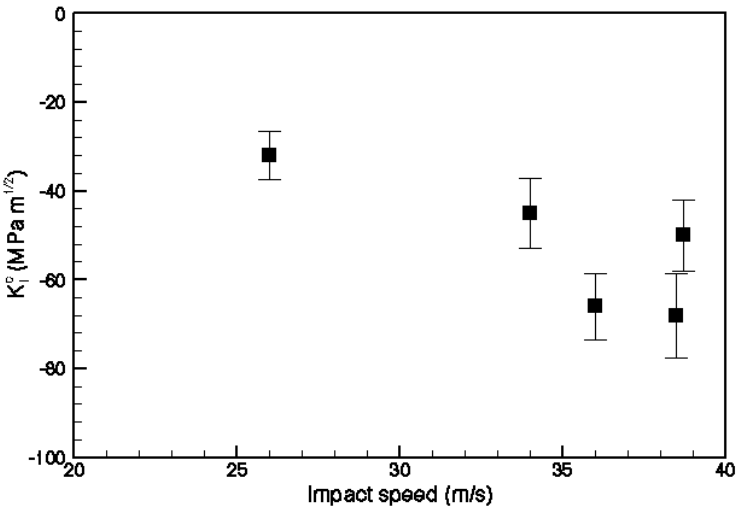

Fig. 19. K_I at the time of shear band initiation as a function of impact speed.

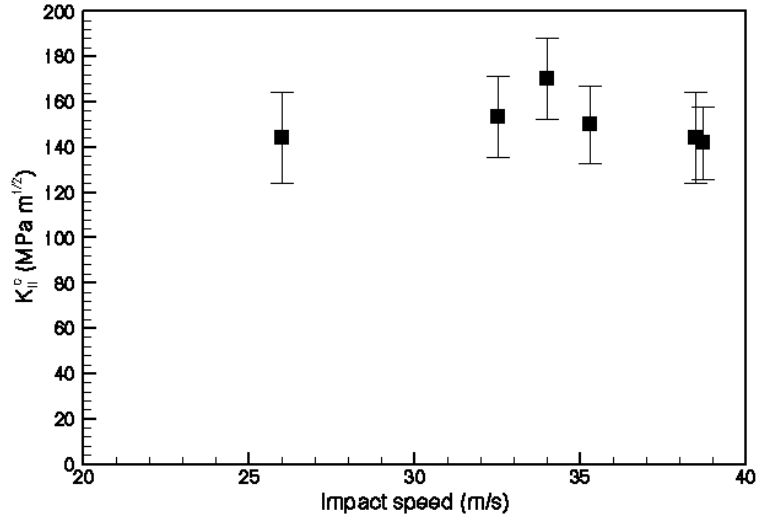

Fig. 20. K_{II} at the time of shear band initiation as a function of impact speed.

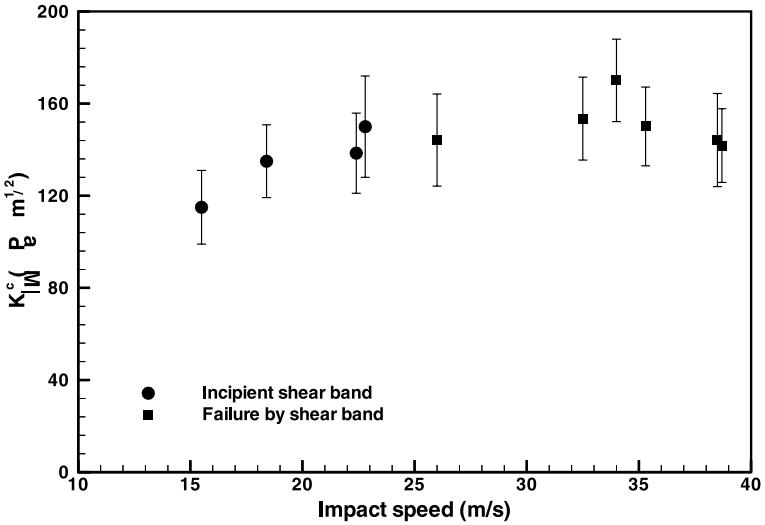

Fig. 21. Critical K_{II} for shear band initiation.

ing its initiation. Figs. 23 and 24 show the advance of the shear band and its velocity in five different experiments. In order to obtain the velocity plot, every set of three consecutive points in Fig. 23 is fitted with a second order polynomial and the slope of this polynomial at its mid point is taken to be the velocity at that point. The velocities computed have an uncertainity of ± 80 m/s. The shear band velocity can be seen to be highly transient and a function of the impact speed. In all but one experiment, the band arrests momentarily at about 30 μs, before accelerating to high speeds. Such transient behavior, not observed in the previous similar investigations (Zhou et al., 1996a), could be because of the different boundary conditions used here. The maximum shear band speed observed here is about 1100 m/s. Freund et al. (1985) estimated the speed of a shear band in certain

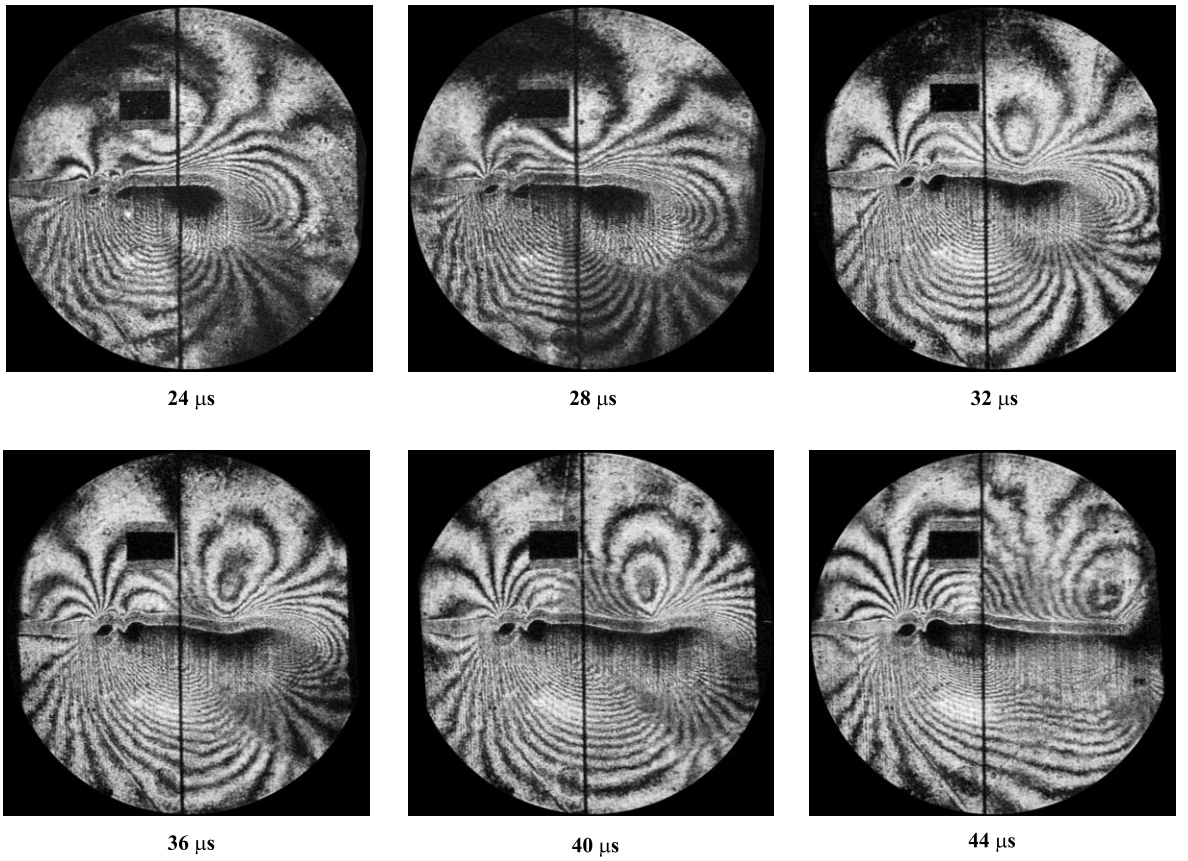

Fig. 22. A sequence of CGS images showing shear band propagation.

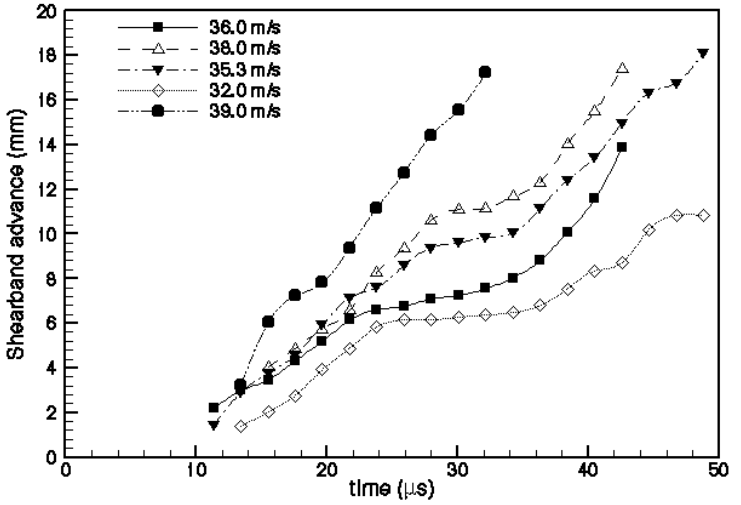

Fig. 23. Shear band advance as a function of time.

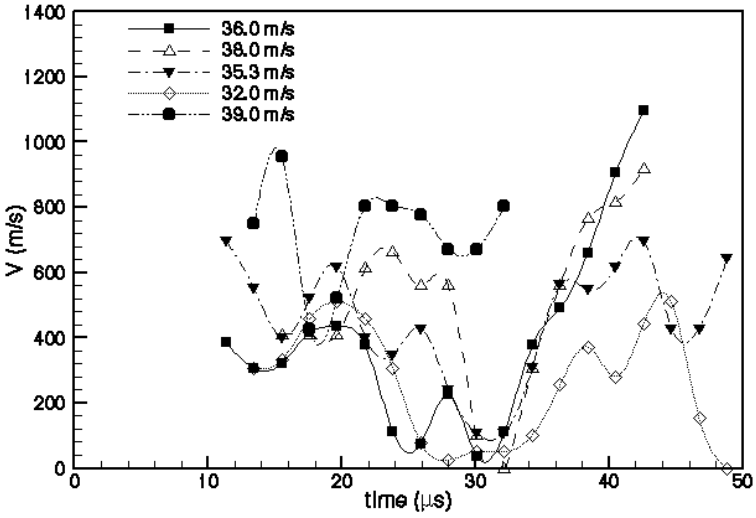

Fig. 24. Shear band velocity as a function of time.

steels to be 0.57 C_S, which is about 1700 m/s. Though the positive slope of the curves in Fig. 24 suggests increasing speeds, further investigations are necessary to determine the limiting speed for a shear band.

3.6. Crack initiation under mixed mode loading

In the experiments, where the impact speed was less than 26 m/s, the crack initiated at an angle to the crack direction, after several wave reflections. This angle is determined by the mode mixity at the time of crack initiation. Similarly, when the impact speed was only slightly above 26 m/s, a shear band initiated at the crack tip, propagated a few millimeters and arrested within the optical field of view. In such cases, the CGS images capture the subsequent development of mixed mode field at the arrested shear band tip, leading to an opening crack initiating at an angle to the initial crack direction. Thus, the current experiments provide an opportunity to investigate the dynamic crack initiation behavior under mixed mode conditions. Fig. 25 shows results from five experiments. The mode mixity is plotted as the abscissa, represented by the mixity parameter $\tan^{-1}(K_{II}/K_I)$ and the crack initiation angle (α) is plotted as the ordinate. The discrete points are the experimental results. The solid line represents the He and Hutchinson (1989) maximum energy release rate criterion and the dashed line represents the local pure mode I criterion. Though the models predict a consistently higher value for the crack initiation angle than what was observed in the experiments, the agreement can be described as reasonable, given the errors in measuring the stress intensity factors.

3.7. Micrographs of shear bands

Fractured specimens were examined using an optical microscope to study the features of the shear bands such as its width, trajectory, etc. Specimens for microscopy were prepared by cutting small samples from the area of interest using EDM. Surface of interest was then polished down to 0.25 μm, followed by etching with 2% nital solution. Fig. 26 is a photograph of an arrested shear band in the specimen. The shear band is revealed as a white stripe. This white band represents the area where the temperature increase was high enough to cause a solid–solid phase transformation. The thickness of the band is about 40 μm. Fig. 27 shows a scanning electron microscope (SEM) image of the specimen surface that failed by shear band propagation. The image shows elongated voids, with sheared edges that are characteristic of

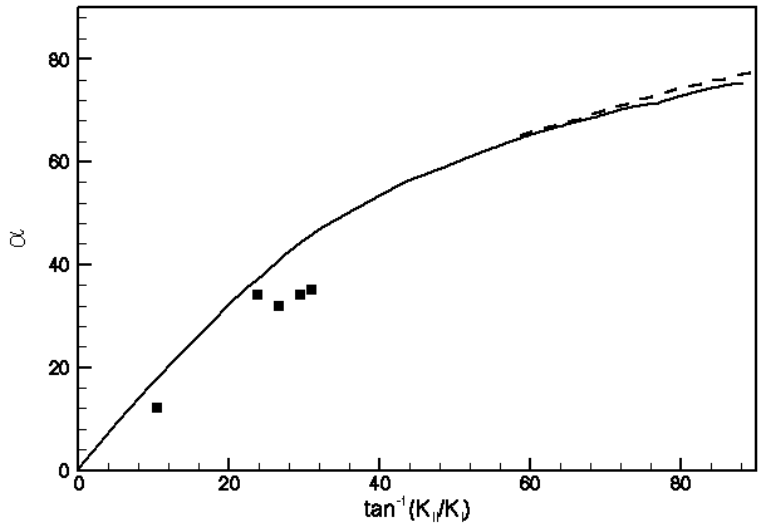

Fig. 25. Mixed mode crack initiation criterion: a comparison with analytical models.

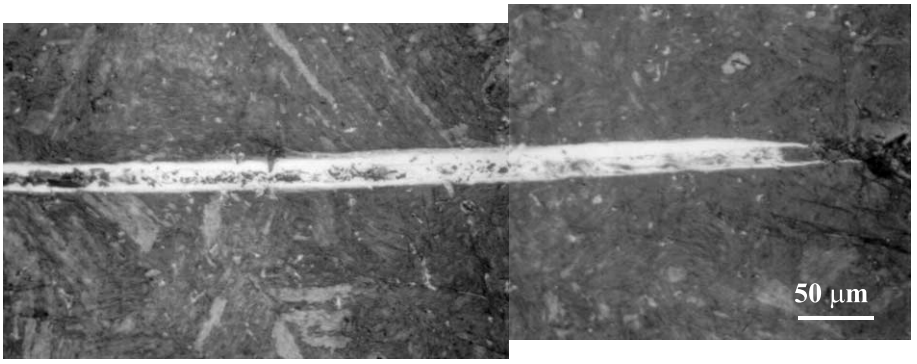

Fig. 26. An optical micrograph of an arrested shear band.

such a failure mode. The presence of voids reveals the development of triaxial tensile stresses that led to void growth and eventual fracture.

Meyers (1994) has made an interesting observation about the possibility of shear band branching, by presenting a micrograph of a shear band that showed a bifurcation. Here we report some of our observations that support such a possibility. Fig. 28 shows three micrographs that show possible shear band bifurcation. In the first two, the left edges are the failure paths, caused by a propagating shear band. The third image is taken from an arrested shear band. The branching behavior is clearly seen in all three cases. To our knowledge, currently there is no theoretical framework to explain such a phenomenon, and we feel that this interesting observation requires further investigation to understand the conditions under which such a bifurcation can take place.

3.8. Temperature measurement

3.8.1. Temperature field at the crack tip

One of the objectives of imaging the temperature field was to visualize the development of the mode II plastic zone at the tip of the initial crack

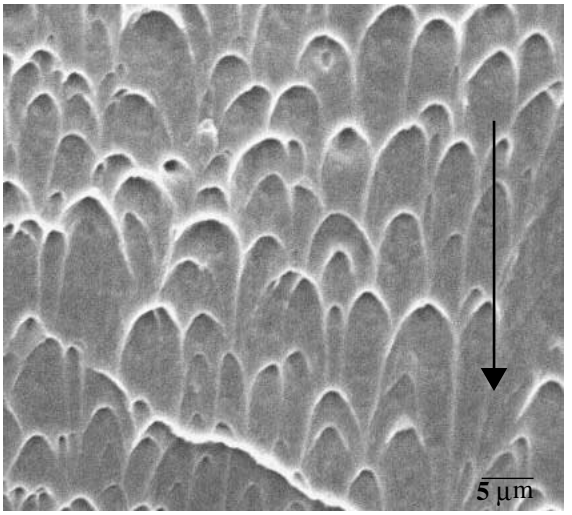

Fig. 27. An SEM image of the fracture surface that failed by shear banding. Arrow shows the crack propagation direction.

and to observe its evolution, through further localization, into a shear band. The IR camera was focussed at the tip of the fatigue crack as illustrated on the left-hand side of Fig. 29. The impact speed was about 35 m/s. Fig. 29 also shows a sequence of thermal images revealing the development of the temperature field as a function of time. It should be remembered that the actual data is collected at 64 discrete points. The images shown here are the projections of contour lines drawn on a surface fitted through the 64 points in the x_1, x_2 and temperature rise, ΔT, space. The black lines on these images were artificially superimposed to represent the approximate location of the initial crack tip. The position of the crack was inferred from the temperature patterns. Plasticity gradually builds up, with the characteristic shape of a mode II dominated plastic zone. Starting at about 21 μs, the central hot region extends to the right, as indicated by the contour lines, signifying the process of shear localization. The measured highest temperature rise within the plastic zone when this happened was at least 80 K. Since each detector averages temperature rise over an area of 110 μm × 110 μm, spatial features smaller than

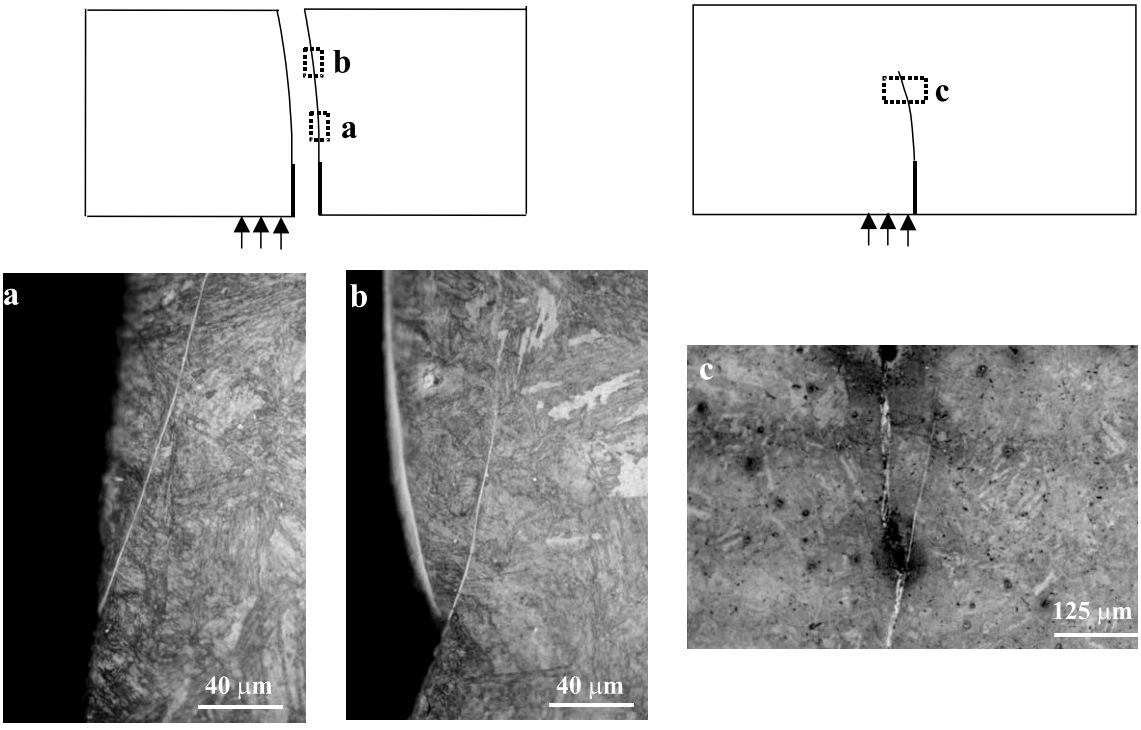

Fig. 28. Optical micrographs of possible shear band bifurcation.

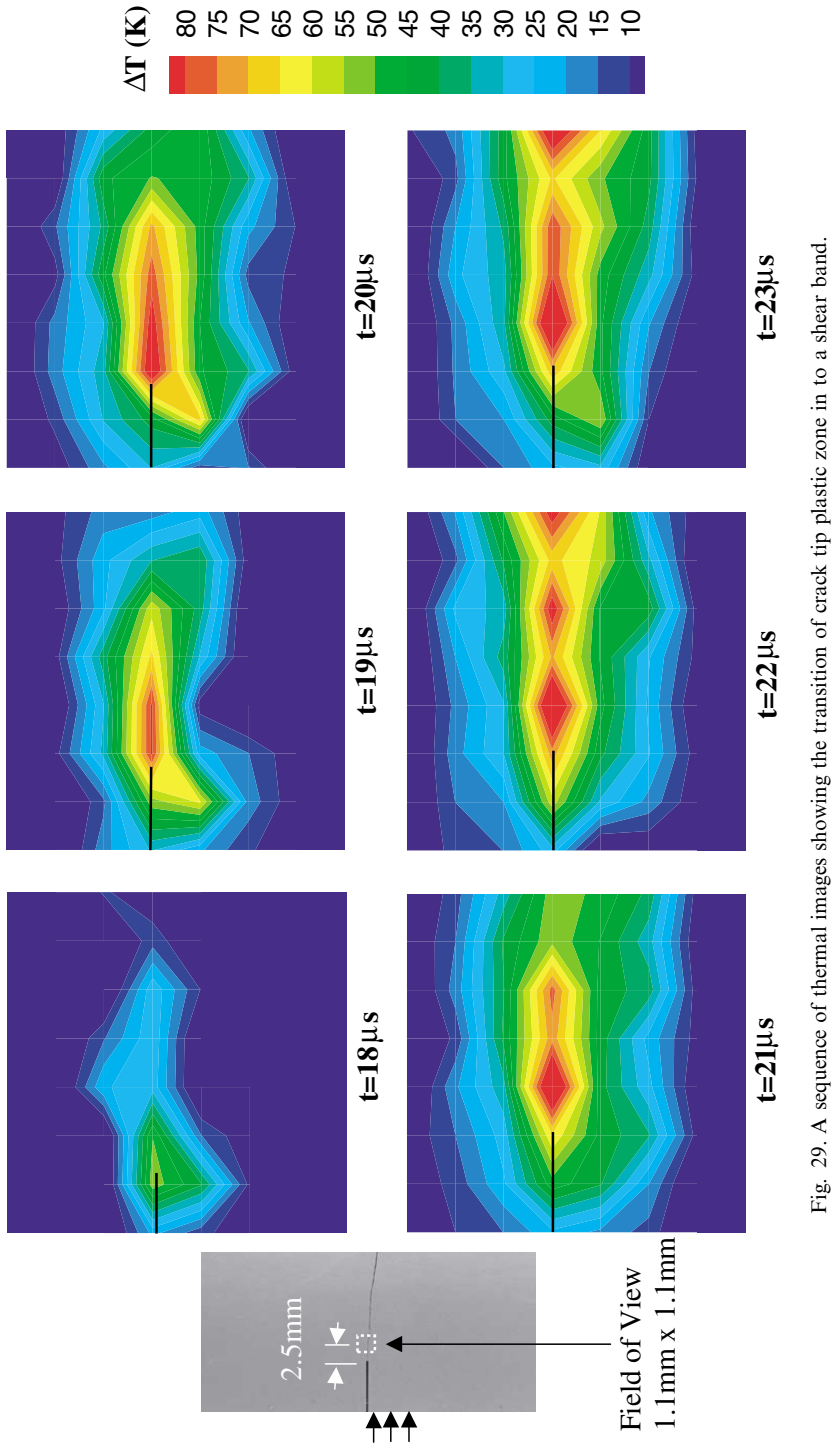

Fig. 29. A sequence of thermal images showing the transition of crack tip plastic zone in to a shear band.

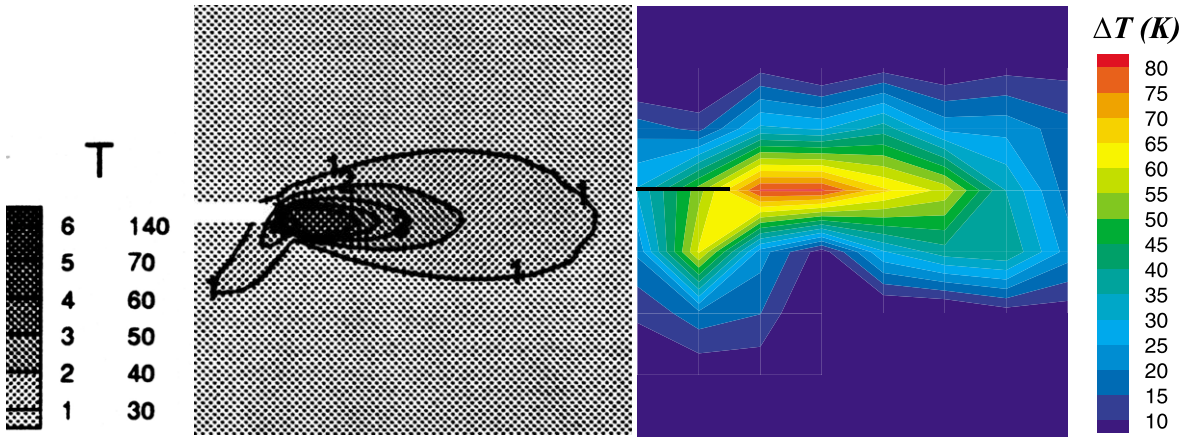

Fig. 30. A comparison of the size and shape of the crack tip plastic zone with numerical solution of Needleman and Tvergaard (1995). (Left figure reprinted from Int. J. Solid. Struct., A. Needleman, V. Tvergaard, Analysis of a brittle-ductile transition under dynamic shear loading, 2571–2570, Copyright 1995, with permission from Elsevier Science.)

this can not be resolved in these measurements. This is the first time that such 2-D thermal images were obtained that clearly capture the transition of the initial crack tip plastic zone into a shear band.

A specific feature of interest here is the shape of the plastic zone prior to shear localization. In the numerical analyses of Needleman and Tvergaard (1995) and Ravi-Chandar (1995), it was observed that the plastic zone was elongated ahead of the crack and it also possessed a short, tail like extension on the side of impact, at about 135° to the crack line. The current IR measurement was able to resolve such features, as illustrated in Fig. 30. This figure shows a qualitative comparison between the simulations of Needleman and Tvergaard (1995) and our current experimental results of the temperature rise within the plastic zone. The two pictures are shown at the same size scale. The comparison is for nominally the same impact speed and at the same time after impact. The difference lies in the material properties. The steel used in the current investigation is about 40% stronger than the one used in their simulations. In spite of this difference, the agreement between the size and shape of the plastic zones is indeed remarkable.

3.8.2. Structure of the tip of a propagating shear band

Next we turn our attention to the temperature field associated with the tip of a propagating shear band. There have been numerous speculations about its existence and the nature of an autonomous stress–strain field associated with it. In order to image the structure of such a propagating shear band tip, the IR camera was focussed at a distance of 3.5 mm ahead of the initial crack tip, in the expected path of shear band propagation. Fig. 31 shows a sequence of temperature images that capture the thermal profile of the tip of the shear band as it propagates across the field of view. 15 μs after impact, a very diffuse temperature front can be seen entering the field of view. The front moves rapidly across the field of view and the temperature increases gradually. The temperature rises by at least 40 K in 4 μs and the gradient of temperature increase is about 5×10^4 K/m along the direction of propagation of the shear band. As noted above, since the spot size is 110 μm, and the width of the shear band is at most 50 μm, the temperature rise measured here is only a lower bound for the actual value. The tip of the first detectable temperature rise was seen to propagate across the field of view at a speed of about 500 m/s. The gradual nature of temperature rise at the front end of the shear band supports the notion of a very diffuse shear band tip, as opposed to a crack tip which carries a strong singularity in the field quantities. The idea of a diffuse tip was first proposed by Gioia and Ortiz (1996). From a bound-

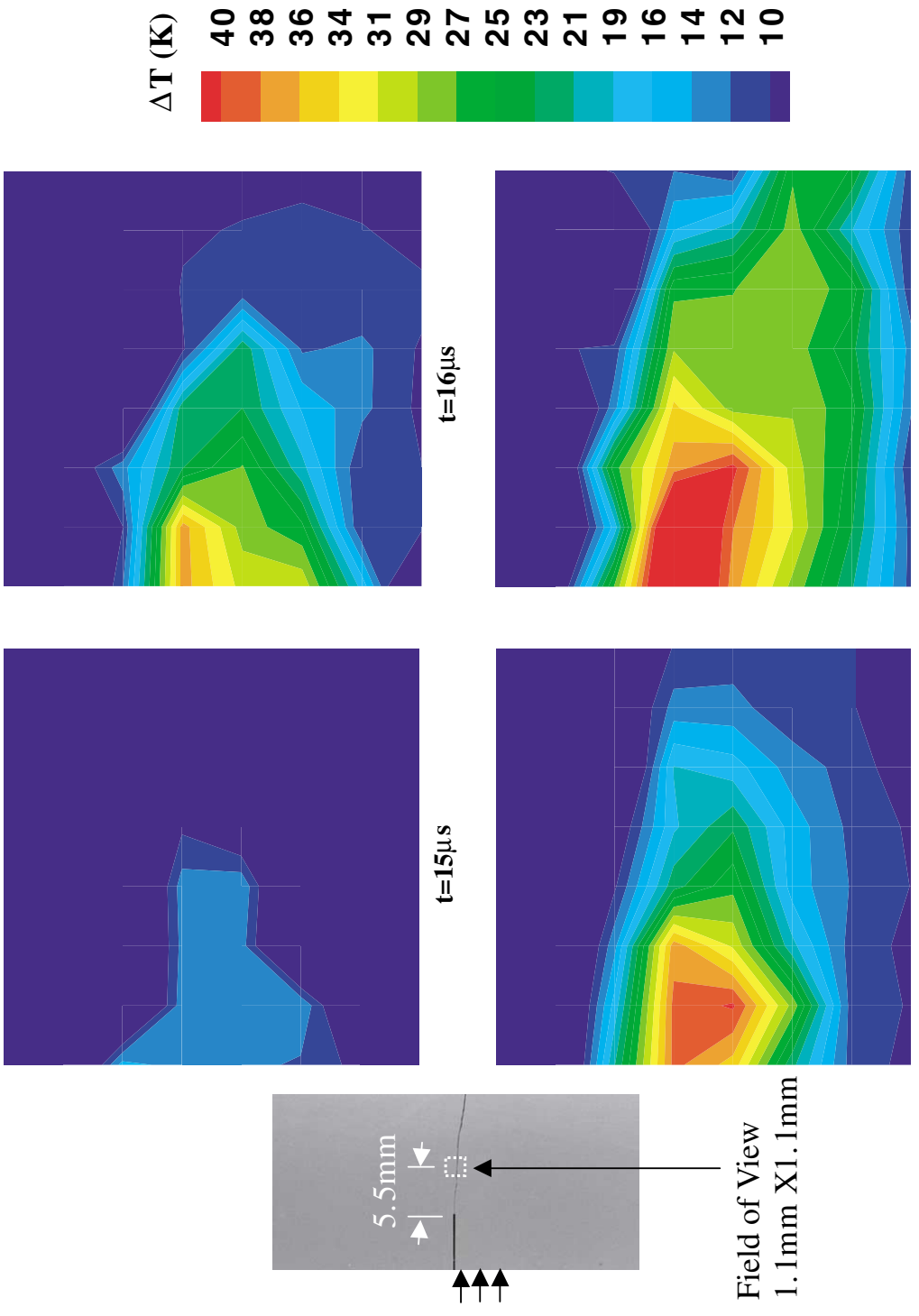

Fig. 31. A sequence of thermal images revealing the structure of the tip of a propagating shear band.

ary layer theory, they introduced the idea of a shear band tip that carries no discontinuities and is characterized by the accumulation of a critical amount of plastic work to render the material behind it unstable by virtue of the change in the nature of its stress strain behavior. The current experimental results appear to support this idea.

3.8.3. Temperature structure along a propagating shear band

As the shear band propagates, the material within the band progressively accumulates large plastic shear strains within short times and the temperatures can quickly reach very high values. Of special interest in this investigation has been the temperature distribution along a well-defined shear band. It has been consistently observed, in all experiments where a propagating shear band was imaged, that the temperature distribution along the band is highly non-uniform, with discrete regions of high temperature, that look like "hot spots." These hot spots are also seen to translate along the length of the band. Fig. 32 shows one such image where the hot spots can be identified easily. In this image the hot spots are spaced at about 250 μm and in general the spacing varied from 250 μm to 1 mm. This observation raises questions about the spatial and temporal nature of shear deformation inside a shear band, which until now has been assumed to be essentially laminar in all the available theoretical models. The high speed images obtained here show the shearing process to be far from laminar and the hot spots observed indicate a possible instability operating at the band width length scale, similar to certain hydrodynamic instabilities observed in fluids. Since in a shear band, a very thin layer of very hot material is subjected to extremely high shear strain rates, the situation may resemble that of a viscous fluid confined between two rigid plates moving parallel to each other, known as the plane Couette flow in the fluid dynamics parlance. Since the

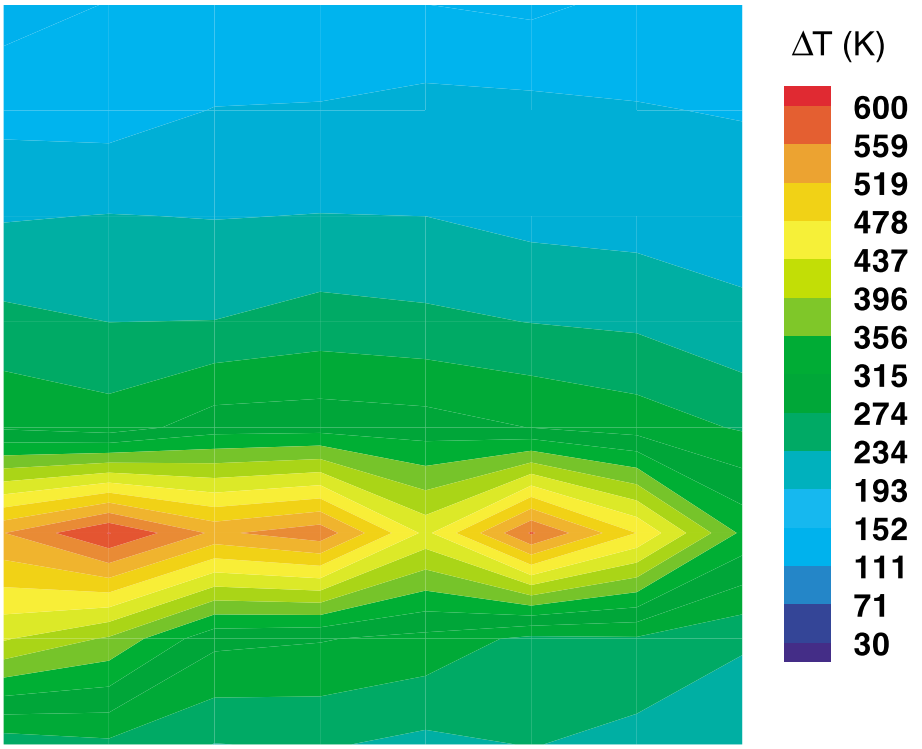

Fig. 32. A thermal image of a shear band showing non-uniform temperature distribution along the length of the band.

plane Couette flow could become unstable and turbulent under certain conditions, it was conjectured that the hot spots observed in the current experiments indicate an instability of the deformation process. This led us to examine the stability characteristics of the plane Couette flow.

It is well known in fluid mechanics that plane Couette flow of inviscid as well as viscous fluids is linearly stable. However, the situation is different if the viscosity of the fluid is a function of temperature since viscous dissipation increases local temperature. The linear stability of plane Couette flow with viscous heating was numerically studied by Sukanek et al. (1973) and later with improved numerical accuracy by Yueh and Weng (1996). It was found that perturbations of finite wave numbers along the flow direction grow unboundedly beyond a critical Reynolds number, leading to eventual turbulence. This lends credence to our notion of the analogy with a flow related instability in a shear band since the temperature rise in a shear band decreases local viscosity of the material. Yet, there are major differences between a shear band and the Couette flow with viscous heating. The shear band temperatures are approximately one-half of the melting temperature of the steel, indicating that the local shear band behavior can not be necessarily approximated by that of a viscous fluid. Indeed, a more appropriate description of the material behavior would be one of a thermo-viscoplastic material.

Motivated by observations at an entirely different length scale, namely, the existence of ductile shear zones with spatial periodicity in the earth's lower crust, where the material is constantly sheared, Molinari and Leroy (1991) conducted a 2-D quasi-static perturbation analysis of a layer of thermo-viscoplastic material subjected to shearing at the boundaries, as shown in Fig. 33. The viscosity of the material they modeled was an exponentially decreasing function of temperature. They investigated the possibility of the existence of any perturbations with a finite wave number in the direction along the band that could become unstable and grow as the deformation proceeds. They found that for certain material properties, such perturbations do exist and they lead to periodic hot spots along the length of the shear band as also

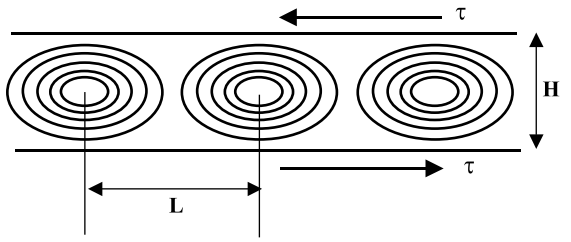

Fig. 33. Linear stability analysis of the deformation of a layer of material subjected to a shear stress. The ellipses are contours of constant temperature, with increasing value towards the center.

illustrated in Fig. 33. These results, although quasi- static, can be used to understand the present case of a shear band since the material used in the current investigation has properties that are close to those of the material used in their analysis. The results of Molinari and Leroy (1991) show that the non-dimensional wave numbers of unstable perturbations range from 0.02 to 0.1, which, using a shear band width of 40 μm (Fig. 26), would mean wavelengths of about 1.2–5.0 mm. In the current experiments, the distance between the hot spots was seen to be between 250 μm and 1.0 mm (Fig. 32), which is lower than the range predicted by their analysis, but well within the order of magnitude, supporting our hypothesis that the observed non-uniform features are related to an instability of laminar flow of the material within the shear band. This finding calls for models that account for such microstructures in order to accurately estimate the energy dissipation in shear bands and to describe the dynamics of shear band formation, growth and arrest. Motivated by the current experimental observations, detailed numerical simulations are currently underway in order to investigate the microstructure of the shear bands using mesh-less numerical schemes (Li et al., 2001a,b).

4. Concluding remarks

Impact experiments have been conducted on single edge notched specimens made of C300 maraging steel to study impact induced failure mode transition by simultaneously employing the optical

technique of CGS and the high speed 2-D thermal imaging. Macroscopically, a failure mode transition from an opening crack to a shear band was observed at a critical impact speed of 26 m/s. However, a closer examination of the initial crack tip area reveals a small arrested shear band even in the experiments with sub-critical impact speed. When the impact speed is below 26 m/s, the band arrests immediately and the crack initiates from the tip of the pre-fatigued crack in opening mode after multiple wave reflections. Measurements of stress intensity factor histories indicate a critical range of values for K_{II} over which a shear band initiates from the crack tip. This supports earlier suggestions of a K_{II} based criterion for shear band initiation. The 2-D thermal images of the shear band initiation and propagation processes present several new observations. The shear band tip is seen to possess a very diffuse structure, with a gradual increase in temperature. A rather surprising finding from this investigation has been the non-uniform temperature distribution along a shear band. This observation has been possible due to the high speed IR camera developed for such applications. All analytical and numerical models of propagating shear bands so far have assumed a laminar deformation for the material within the shear band. New models are required to account for the non-uniform temperature distribution, which directly affects the energy dissipation in a shear band.

Acknowledgements

This work was supported by the Office of Naval Research grant # N00014-95- 1-0453 (Dr. Y.D.S. Rajapakse, project manager) and the engineering research program of the office of Basic Energy Sciences at the Department of Energy through grant No. DE-F603-95ER14560 (Dr. Robert Price, Project officer). Additional funding for the development of the infrared camera was provided by the National Science Foundation through the Center for Quantitative Visualization at Caltech (Professor M. Gharib, Director). We are also pleased to acknowledge the contributions of Professor A.T. Zehnder, Cornell University, for his pivotal role in developing the high speed IR camera. PRG acknowledges many useful discussions with Dr. David M. Owen, Caltech throughout this work.

References

Bai, Y.L., 1982. Thermo-plastic instability in simple shear. J. Mech. Phys. Solids 30, 195–207.

Bai, Y.L., Dodd, B., 1992. Adiabatic Shear Localization: Occurrence, Theories and Applications. Pergamon Press, Oxford.

Chen, L., Batra, R.C., 1998a. Shear instability direction at a crack-tip in a thermoviscoplastic body. Theor. Appl. Fract. Mech. 29, 33–40.

Chen, L., Batra, R.C., 1998b. Analysis of material instability at an impact loaded crack tip. Theor. Appl. Fract. Mech. 29, 213–217.

Chen, L., Batra, R.C., 1998c. Material instability criterion near a notch-tip under locally adiabatic deformations of thermoviscoplastic materials. Theor. Appl. Fract. Mech. 30, 153–158.

Clifton, R.J., 1980. Material response to ultra high loading rates. NRC Report No. 356, US National Material Advisory Board.

Clifton, R.J., Duffy, J., Hartley, K.A., Shawki, T.G., 1984. On critical conditions for shear band formation at high strain rates. Script. Metall. 18, 443–448.

Costin, L.S., Crisman, E.E., Hawley, R.H., Duffy, J., 1979. On the localization of plastic flow in mild steel tubes under torsional loading. In: Harding, J. (Ed.), Second Conference on the Mechanical Properties of Materials at High Rates of Strain. The Institute of Physics, London, pp. 90–100.

Freund, L.B., Wu, F.H., Toulios, M., 1985. Initiation and propagation of shear band in antiplane shear deformation. In: Proceedings of the Considere Memorial Symposium. Presse de l'Ecole Nationale des Ponts et Chaussees, pp. 125–143.

Gioia, G., Ortiz, M., 1996. The two-dimensional structure of dynamic boundary layers and shear bands in thermoviscoplastic solids. J. Mech. Phys. Solids 44, 251–292.

Grady, D.E., 1992. Properties of an adiabatic shear band process zone. J. Mech. Phys. Solids 40, 1197–1215.

Grady, D.E., 1994. Dissipation in adiabatic shear bands. Mech. Mater. 17, 289–293.

Guduru, P.R., Singh, R.P., Ravichandran, G., Rosakis, A.J., 1998. Dynamic crack initiation in ductile steels. J. Mech. Phys. Solids 46, 1997–2016.

Hartley, K.A., Duffy, J., Hawley, R.H., 1987. Measurement of the temperature profile during shear band formation in steels deforming at high strain rates. J. Mech. Phys. Solids 35, 283–301.

He, M.-Y., Hutchinson, J.W., 1989. Kinking of crack out of an interface. J. Appl. Mech. 56, 270–278.

Hodowany, J., Ravichandran, G., Rosakis, A.J., Rosakis, P., 2000. Partition of plastic work into heat and stored energy in metals. Exper. Mech. 40, 113–123.

Kallivayalil, J.A., Zehnder, A.T., 1994. Measurement of the temperature field induced by dynamic crack growth in beta-C titanium. Int. J. Fract. 66, 99–120.

Kalthoff, J.K., Winkler, S., 1988. Failure mode transition at high rates of loading. In: Chiem, C.Y., Kunze, H.D., Meyer, L.W., (Eds.), Proceedings of the International Conference on Impact Loading and Dynamic Behaviour of Materials. Deutsche Gesellschaft fur Metallkunde, pp. 43–56.

Lee, Y.J., Freund, L.B., 1990. Fracture initiation due to asymmetric impact loading of an edge cracked plate. J. Mech. Phys. Solids 57, 104–111.

Li, S., Liu, W-K., Hao, W., Rosakis, A.J., 2001a. Simulations of dynamic shear band propagation. Part I: Brittle to ductile transition. Submitted to Int. J. of Solid. Struct.

Li, S., Liu, W-K., Rosakis, A.J., Guduru, P.R., 2001b. Simulations of dynamic shear band propagation. Part II: Micro-structure of adiabatic shear band. In preparation.

Li, Z., Lambros, J., 2000. Dynamic thermomechanical behavior of fiber reinforced composites. Composites, Part A – Appl. Sci. Manufact. 31, 537–547.

Marchand, A., Duffy, J., 1988. An experimental study of the formation process of adiabatic shear bands in a structural steel. J. Mech. Phys. Solids 36, 251–283.

Mason, J.J., Lambros, J., Rosakis, A.J., 1992. The use of a coherent gradient sensor in dynamic mixed mode fracture mechanics experiments. J. Mech. Phys. Solids 40, 641–661.

Mason, J.J., Rosakis, A.J., 1993. On the dependence of the dynamic crack-tip temperature fields in metals upon crack-tip velocity and material parameters. Mech. Mater. 16, 337–350.

Meyers, M.A., 1994. Dynamic Behavior of Materials. Wiley, New York.

Molinari, A., Clifton, R.J., 1987. Analytical characterization of shear localization in thermoviscoplastic materials. J. Appl. Mech. 54, 806–812.

Molinari, A., Leroy, Y.M., 1991. Structures in shear zones due to thermal effects. C.R. Acad. Sci. Paris, Serie II, 313, 7–13.

Moss, G.L., 1981. Shear strains, strain rates and temperature changes in adiabatic shear bands. In: Meyers, M.A., Murr, L.E. (Eds.), Shock Waves and High-Strain-Rate Phenomena in Metals. Plenum Press, New York, pp. 299–312.

Moss, G., Pond, R.B. Sr., 1975. Inhomogeneous thermal changes in copper during plastic elongation. Metall. Trans. 6A, 1223–1235.

Needleman, A., Tvergaard, V., 1995. Analysis of a brittle–ductile transition under dynamic shear loading. Int. J. Solid. Struct. 32, 2571–2590.

Ravi-Chandar, K., 1995. On the failure mode transition in polycarbonate under dynamic mixed mode loading. Int. J. Solid. Struct. 32, 925–938.

Ravi-Chandar, K., Lu, J., Yang, B., Zhu, Z., 2000. Failure mode transitions in polymers under high strain rate loading. Int. J. Fract. 101, 33–72.

Recht, R.F., 1964. Catastrophic thermoplastic shear. J. Appl. Mech. 31, 189–193.

Rittel, D., Levin, R., 1998. Mode-mixity and dynamic failure mode transitions in polycarbonate. Mech. Mater. 30, 197–216.

Roessig, K.M., Mason, J.J., 1998. Adiabatic shear localization in the impact of edge-notched specimens. Exper. Mech. 38, 196–203.

Rogers, H.C., 1979. Adiabatic plastic deformation. Ann. Rev. Mater. Sci 9, 283–311.

Rosakis, A.J., 1993. Two optical techniques sensitive to gradients of optical path difference: the method of caustics and the coherent gradient sensor (CGS). In: Epstein, J. (Ed.), Experimental Techniques in Fracture. VCH, New York, pp. 327–425.

Shawki, T.G., Clifton, R.J., 1989. Shear band formation in thermal viscoplastic materials. Mech. Mater. 8, 13–43.

Sukanek, P.C., Goldstein, C.A., Laurence, R.L., 1973. The stability of plane Couette flow with viscous heating. J. Fluid. Mech. 57, 651–670.

Tippur, H.V., Krishnaswamy, S., Rosakis, A.J., 1990. Coherent gradient sensor for crack tip deformation measurements: analysis and experimental results. Int. J. Fract. 48, 193–204.

Tippur, H.V., Krishnaswamy, S., Rosakis, A.J., 1991. Optical mapping of crack tip deformations using the method of transmission and reflection coherent gradient sensing: a study of crack tip k-dominance. Int. J. Fract. 52, 91–117.

Wright, T.W., 1987. Steady shearing in a viscoplastic solid. J. Mech. Phys. Solids 35, 269–282.

Wright, T.W., 1995. Scaling laws for adiabatic shear bands. Int. J. Solids Struct. 32, 2745–2750.

Wright, T.W., Ockendon, H., 1992. A model for fully formed shear bands. J. Mech. Phys. Solids 40, 1217–1226.

Wright, T.W., Ravichandran, G., 1997. Canonical aspects of adiabatic shear bands. Int. J. Plasticity 13, 309–325.

Wu, F.H., Freund, L.B., 1984. Deformation trapping due to thermoplastic instability in one-dimensional wave-propagation. J. Mech. Phys. Solids 32, 119–132.

Yueh, C-S., Weng, C-I., 1996. Linear stability analysis of plane Couette flow with viscous heating. Phys. Fluids 8, 1802–1813.

Zehnder, A.T., Guduru, P.R., Rosakis, A.J., Ravichandran, G., 2000. Million frames per second infrared imaging system. Rev. Sci. Instrum. 71, 3762–3768.

Zehnder, A.T., Ramamurthy, A.C., Bless, J., Brar, N.S., 1993. Stone impact damage to automotive paint finishes – measurement of temperature rise due to impact. Int. J. Impact. Eng. 13, 133–143.

Zehnder, A.T., Rosakis, A.J., 1991. On the temperature distribution at the vicinity of dynamically propagating cracks in 4340 steel. J. Mech. Phys. Solids 93, 385–415.

Zehnder, A.T., Rosakis, A.J., 1992. A note on the use of high speed infrared detectors for the measurement of temperature fields at the vicinity of dynamically growing cracks in 4340 steel. J. Appl. Mech. 59, 450–452.

Zener, C., Hollomon, J.H., 1944. Effect of strain rate upon plastic flow of steel. J. Appl. Phys. 15, 22–32.

Zhou, M., Ravichandran, G., Rosakis, A.J., 1996a. Dynamically propagating shear bands in impact-loaded prenotched plates – I. Experimental investigations of temperature signatures and propagation speed. J. Mech. Phys. Solids 44, 981–1006.

Zhou, M., Ravichandran, G., Rosakis, A.J., 1996b. Dynamically propagating shear bands in impact-loaded prenotched plates – II. Numerical simulations. J. Mech. Phys. Solids 44, 1007–1032.